# MINIMUM IMAGE SIZE FOR PHASE ERROR CORRECTION USING PHASE GRADIENT AUTOFOCUS ON SYNTHETIC APERTURE RADAR IMAGES

By

CAMERON CARROLL

Bachelor of Science in Electrical Engineering

Oklahoma State University

Stillwater, Oklahoma

2012

Submitted to the Faculty of the
Graduate College of the
Oklahoma State University
in partial fulfillment of
the requirements for
the Degree of
MASTER OF SCIENCE
May, 2015

MINIMUM IMAGE SIZE FOR PHASE ERROR CORRECTION USING PHASE GRADIENT AUTOFOCUS IN SYNTHETIC APERTURE RADAR IMAGES

Thesis Approved:

Dr. Jim West

Thesis Adviser

Dr. Damon Chandler

Dr. George Scheets

Cameron Carroll

Date of Degree: MAY, 2015

Title of Study: MINIMUM IMAGE SIZE FOR PHASE ERROR CORRECTION USING PHASE GRADIENT AUTOFOCUS IN SYNTHETIC APERTURE RADAR IMAGES

Major Field: ELECTRICAL ENGINEERING

Abstract:

Synthetic aperture radar (SAR) is used for imaging large patches of earth's surface; however, these images suffer from phase errors induced by demodulation errors. These demodulation error are caused by uncompensated fluctuations in the flight path and atmospheric irregularities which cause unknown delays for the returned signal. Phase errors cause the resulting image to blur along the dimension parallel to the flight path, and must be corrected in order to produce a high resolution radar image. This paper attempts to find a minimum image size for which phase gradient autofocus (PGA) can effectively be used to correct phase errors. To measure the accuracy of the correction two metrics are used: average coherence after coherent change detection (CCD) and mean absolute error (MAE) of the estimated phase error compared to the applied phase error.

TABLE OF CONTENTS

Chapter Page

# LIST OF FIGURES

Figure Page

Figure Page

Figure Page

# CHAPTER I

## INTRODUCTION

Synthetic aperture radar (SAR) is a radar imaging technique used to achieve fine resolution in two dimensions, range and cross-range or *azimuth*, without the need for large impractical antennas. Spotlight mode SAR, the collection method used in this thesis, achieves fine resolution in both dimensions by continuously aiming an antenna mounted on a platform, either plane or satellite, at the center of a patch of earth perpendicular to the flight path. An image can be formed by processing the phase histories of the return pulses. The next two sections describe an overview of the processing required to form a SAR image from the collected phase history data. In later sections the dimension perpendicular to the flight path is range and the dimension parallel to the flight path is azimuth.

During data collection it is necessary to know the amount of time a signal takes to go from the platform to the center of the patch in order to demodulate the signal. This is known demodulation time. Currently it is not possible to know the exact demodulation time throughout the entire data collection process which causes errors in the return data. Specifically, the inaccuracies in demodulation time of returned pulses cause phase errors in the data that must be corrected before a useful image can be created. These phase errors effectively blur the image in the azimuth dimension and depending on the size of the error can make the image unusable. Many autofocus algorithms have been proposed to correct for these phase errors, such as, Phase Gradient Autofocus (PGA) [1], Minimum Entropy [2], and a Multichannel Approach [3]. The autofocus

technique discussed in this paper will be PGA which is the most effective and widely used autofocus technique available.

Due to processing limitations it may be beneficial to use a relatively small image size to cut down on processing time or the image data may be limited. If an image is too small, however, PGA may not be able to properly estimate the phase error. In an urban scene or a scene with multiple strong reflectors PGA may still work on a small image, but on a rural scene with minimal structure i.e. uniform clutter PGA will fail to focus the image. Therefore, for many applications knowing a minimum image size to use with PGA would be beneficial.

The scope of this paper is to determine a technique to measure the accuracy of PGA's phase error estimate and compare results of the PGA for different image sizes. Chapter II gives an overview of SAR, chapter III discusses the causes of phase errors, their correction, and ways to measure the corrections accuracy, chapter IV describes the numerical experiments performed, and chapter V gives the conclusions. The chapter II discussions and equations are adapted from [1].

# CHAPTER II

## SAR OVERVIEW

The following overview is adapted from [1].

### Range Resolution

Most modern imaging radar systems employ a linear FM chirp waveform to achieve power efficient fine range resolution. An example of a linear FM chirp is shown in Figure 1. A linear FM chirp is described by:

$$s(t) = rect(t) * Re\{e^{j(\omega_0 t + \alpha t^2)}\}, \quad (1)$$

where s(t) is the linear FM chirp waveform, $\omega_0$is the radar center frequency, and $\alpha$ is the chirp rate.

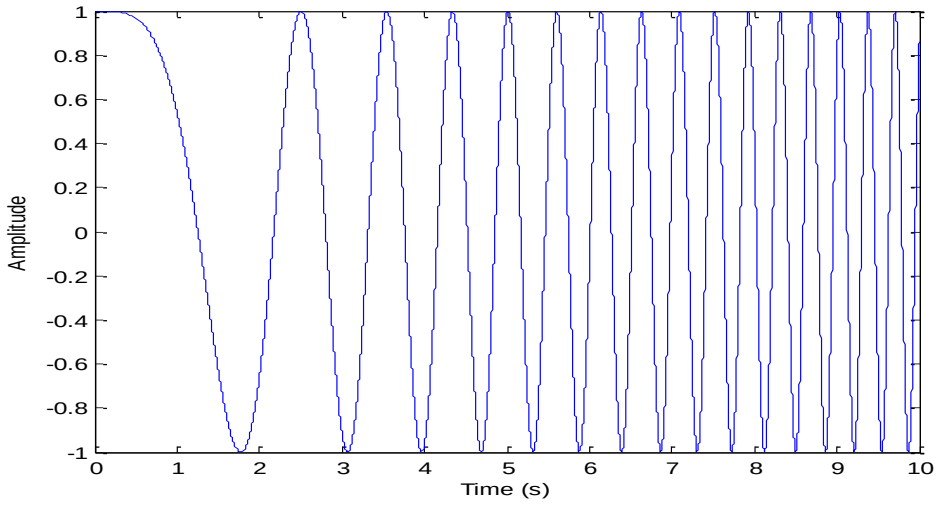


Figure 1: Linear FM Chirp

A waveform with a large bandwidth is desired because a larger bandwidth means a finer range resolution [1]. A chirped signal is used to increase the signal to noise ratio for a desired resolution and peak power. This occurs because the bandwidth of a chirped signal is directly proportional to the signal's duration, so the bandwidth can be controlled by either the chirp rate or the signal duration. The equation for bandwidth, B, of a chirped signal is

$$B = \frac{\alpha \tau_p}{\pi}, \tag{2}$$

where $\tau_p$ is the duration of the pulse. This quality of a chirped waveform is different from an unchirped pulse whose bandwidth is inversely proportional to pulse duration.

The equation for range resolution, $\rho_r$, is

$$\rho_r = \frac{c}{2B} = \frac{c\pi}{2\alpha\tau_p}, \tag{3}$$

where c is the speed of light. From equation (3) there are two values that can be changed to achieve a finer range resolution. By increasing either the chip rate or the chirp duration the resolution will improve and make it possible to create an image where smaller objects are resolvable.

The signal received after its round trip journey to the designated ground patch being imaged is a superposition of scaled and shifted versions of the transmitted signal that encodes the scene reflectivity. In other words, each reflector in the scene is excited by the incoming wave and reflects a scaled and phase shifted version of the transmitted wave back to the antenna, based on the material of the object, its orientation, radar cross section, etc. The receive antenna sees the sum of all the reflected waves.

Figure 2 is an illustration of the collection geometry for a typical SAR system.

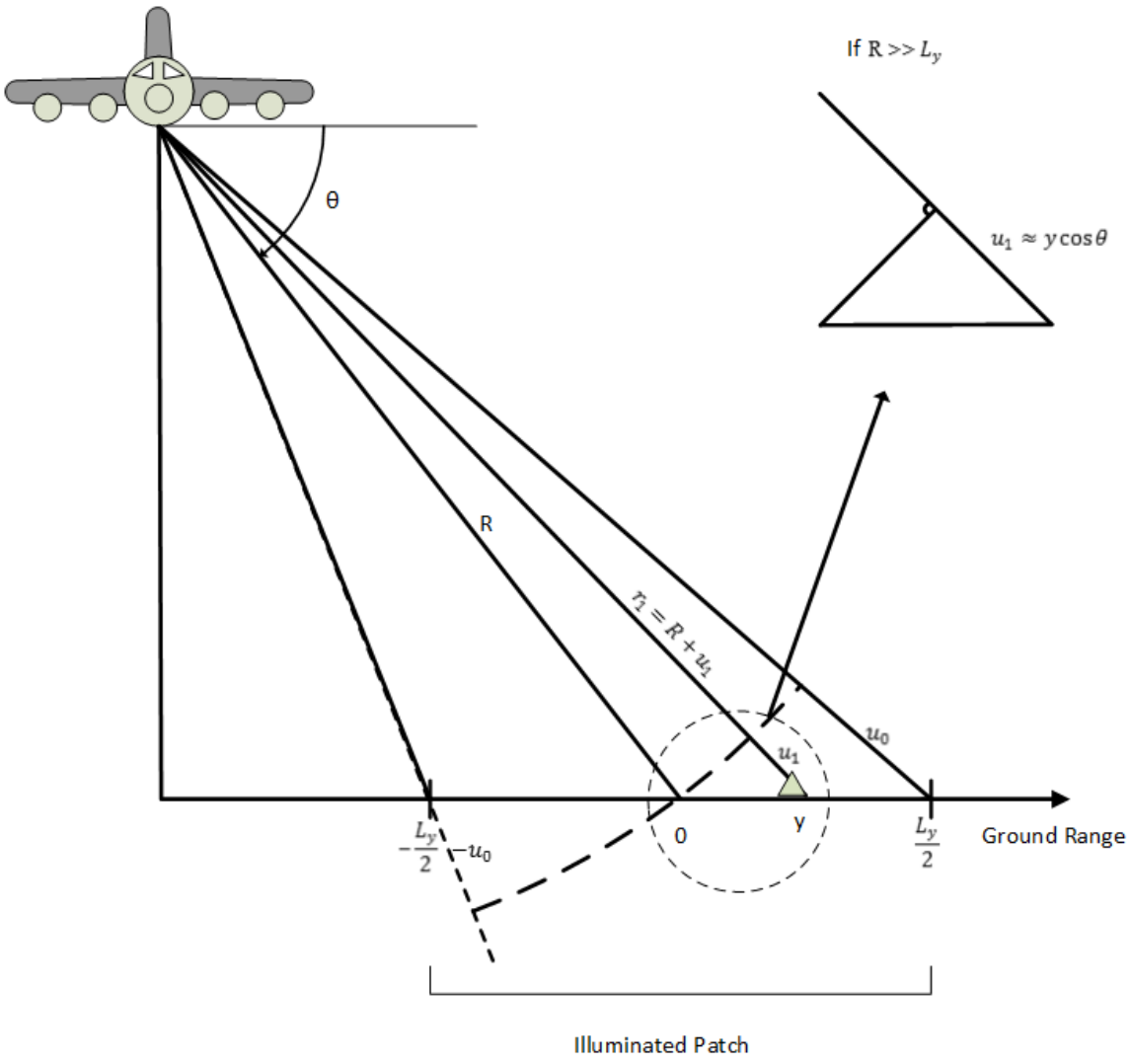


Figure 2 Collection Geometry [adapted from 1]

The round trip time from the platform to the center of the patch is

$$\tau_0 = \frac{2R}{c}. \tag{4}$$

$\tau_0$ is used as a reference to demodulate the returned signal in a typical spot-light mode SAR system. Therefore, it is beneficial to reference the round trip time to any reflector in the scene to the time to the scene center.

$$\tau(u) = \tau_0 + \frac{2u}{c}, \tag{5}$$

where u is the difference between the slant range to a particular target and the slant range to the center of the patch and is bounded by $-u_0 \leq u \leq u_0$ where $u_0 = \frac{L_y}{2}\cos\theta$. As long as R >> $L_y$, the angle θ for the center of the patch can be used for all targets within the scene.

The returned signal then, is described by

$$r(t) = \mathrm{A}\boldsymbol{Re}\left\{\int_{-u_0}^{u_0} g(u)e^{j\left[\omega_0\left(t-\tau_0-\frac{2u}{c}\right)+\alpha\left(t-\tau_0-\frac{2u}{c}\right)^2\right]}du\right\}, \tag{6}$$

where A is a scaling factor to account for attenuation, $\omega_0$ is the radar center frequency, and g(u) is the complex scene reflectivity function.

In order to get the scene reflectivity function from the returned signal, r(t) is processed using a deramp procedure. The deramp process deconvolves the transmitted signal s(t) from the received signal r(t) to obtain the scene reflectivity g(u). There are two main steps to deramp the returned signal; quadrature (IQ) demodulation followed by Fourier transform. IQ demodulation involves mixing the return signal with an in-phase and a quadrature version of a reference signal. In this case the transmitted chirped delayed by $\tau_0$ is the reference signal used. Once the signals are mixed both the in-phase and quadrature components are lowpass filtered leaving the return signal $r_b$. A complex representation for the demodulated return signal is

$$r_b(t) = \frac{A}{2}\int_{-u_0}^{u_0} g(u)e^{-j\left[\frac{2u}{c}(\omega_0+2\alpha(t-\tau_0))\right]}du, \tag{7}$$

By substituting

$$U = \frac{2}{c}[\omega_0 + 2\alpha(t-\tau_0)], \tag{8}$$

$r_b(t)$ becomes

$$r_b(U) = \frac{A}{2}\int_{-u_0}^{u_0} g(u)e^{-juU}du. \tag{9}$$

Then by taking a Fourier transform of equation (9), also known as range compression, the complex scene reflectivity function is resolved in range. Other problems arise, however, when trying to resolve objects located at the same range from the platform which is the subject of the next section.

## Azimuth Resolution

The problem of finding the scene reflectivity expands to two dimensions when attempting to resolve objects along azimuth. Now the goal is to find the scene reflectivity g(x,y) where x is the azimuth dimension and y is the range dimension. Achieving fine azimuth resolution is a problem because for a given pulse the returns from reflectors at the same range from the platform arrive at the antenna at the same time. This means that for a single pulse, reflectors at a constant range from the platform within the antenna beam cannot be resolved i.e. they appear to be one object across azimuth.

Real-aperture radars achieve cross range resolution by using a narrow beam to image the scene. This solution, however, becomes impractical when trying to achieve fine resolution in the azimuth dimension because azimuth beam width is

$$W = \frac{R\lambda}{D}, \tag{10}$$

where R is the range from the platform to the ground, λ is the wavelength, and D is the length of the physical aperture of the antenna [1]. An example effectively demonstrates the impracticality of real-aperture radars for achieving fine azimuth resolution. If resolution of 1m is desired by a radar system that operates at 10 GHz from 10 km away, then

$$D = \frac{10x10^3(.03)}{1} = 300m.$$

This would require an antenna with an aperture of 300m for a course resolution of 1m. This is the main reason for the development of synthetic aperture radars.

SAR imaging radars use signal processing to achieve the effect of a large antenna making fine azimuth resolution realizable. Spotlight-mode SAR, in particular, achieves azimuth resolution by continuously steering an antenna towards a desired patch and processing multiple pulses. Data from a variety of viewing angles are collected and can be used to achieve fine resolution in azimuth. Mathematically the complex reflectivity function from a single return pulse at angle, $\varphi$, can be thought of as an integration of all reflectors that are the same range from the platform or

$$p_{\varphi}(\bar{y}) = \int_{-\frac{L_{\bar{x}}}{2}}^{\frac{L_{\bar{x}}}{2}} g[x(\bar{x},\bar{y}), y(\bar{x},\bar{y})]d\bar{x}, \tag{11}$$

Where $\bar{x}$ is the instantaneous azimuth dimension, $\bar{y}$ is the instantaneous range dimension and $L_{\bar{x}}$ is the length of the patch in the $\bar{x}$ dimension. The coordinate systems are related by the transform

$$\begin{aligned} x &= \bar{x}\cos\varphi - \bar{y}\sin\varphi, \\ y &= \bar{x}\sin\varphi + \bar{y}\cos\varphi, \end{aligned} \tag{12}$$

After IQ demodulation but before applying a Fourier transform a returned pulse is represented by

$$r_b(t) = A\int_{-\frac{L_y}{2}}^{\frac{L_y}{2}} p_{\varphi}(\bar{y})e^{-j[\frac{2y\cos\theta}{c}(\omega_0+2\alpha(t-\tau_0))]}\,d\bar{y}, \tag{13}$$

Where $p_{\varphi}(\bar{y})$ being an integration of a number of targets implies that to acquire information about individual reflectors in the azimuth dimension multiple pulses must be processed.

Each pulse taken from a particular angle, after demodulation but before applying a Fourier transform, corresponds to a line segment of the three dimensional spatial-frequency data. The entire collection process yields a two dimensional ribbon of the scenes spatial-frequency which is the Fourier transform of the scenes complex reflectivity function or G(X,Y). Therefore, to form a complex SAR image each return pulse is deramped and a Fourier transform is taken across the azimuth dimension. The exact details for how this is done are beyond the scope of this paper, however, they are detailed in [1] if the reader requires additional information.

Errors in flight path and atmospheric irregularities add phase errors to the sampled data (the "phase history") which causes blurring across azimuth. The cause of phase errors, their correction, and the accuracy of the correction are the scope of Chapter III.

# CHAPTER III

# PHASE ERRORS: CAUSES, CORRECTION, ACCURACY

## Phase Errors

In order to correctly demodulate a return pulse, the distance from the SAR platform to the center of the patch needs to be known to within a fraction of the wavelength of the radar center frequency. For example, if the radar center frequency is 10 GHz the location of the plane with respect to the patch center would need to be known to within a fraction of 3cm. Modern measuring systems onboard the plane used for position estimation such as gyroscopes, ring lasers, GPS, etc. are not perfect and therefore induce inaccuracies into the system. Due to the location uncertainties of the platform, the demodulations of the return pulses are imprecise which causes phase errors in the phase history that leads to image blurring [1].

### *Mathematical Phase Error Representation*

After interpolating the polar raster into a rectangular grid each column, or azimuth position, in the spatial-frequency domain corresponds to a returned pulse. The phase error varies from pulse to pulse but is considered constant within one pulse. In other words, the phase error changes along azimuth but for each azimuth position every range location has the same phase error. Figure 3 illustrates an example of a phase error across an image.

Mathematically the phase error can be described by

$$\phi(X) = \{\phi_1, \phi_2, \dots, \phi_M\}, \tag{14}$$

where X is the azimuth position and M is the largest azimuth bin.

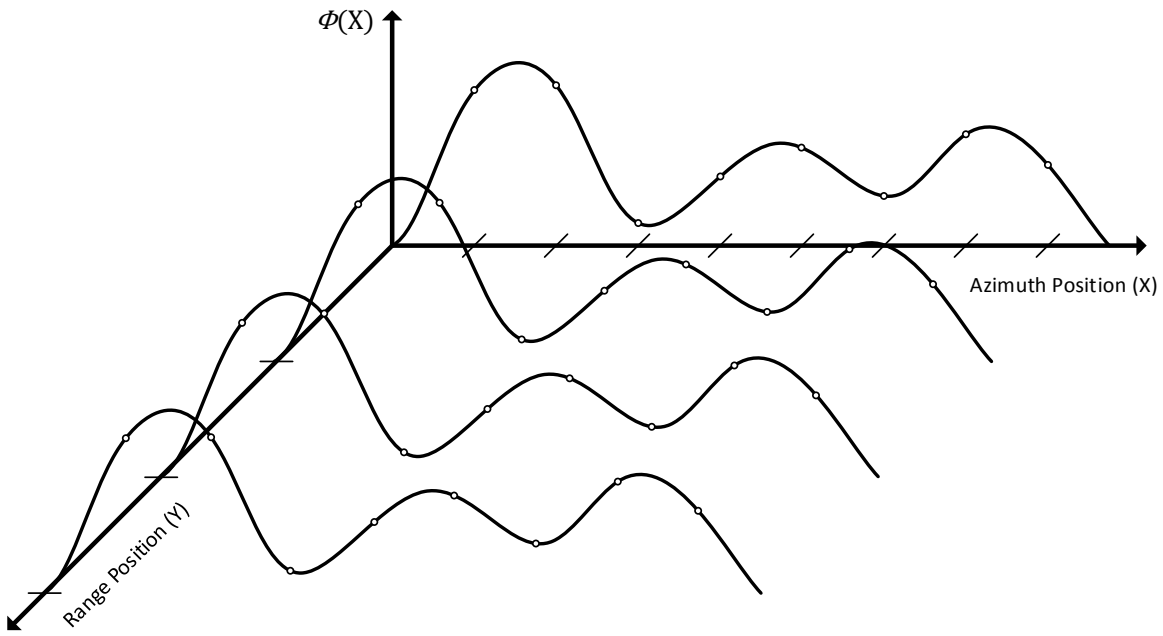


Figure 3 Phase Error across an Image (adapted from [1]).

The corrupted range compressed image samples $\tilde{G}(X, y)$ are then related to the uncorrupted samples $G(X, y)$ by:

$$\tilde{G}(X, y) = G(X, y)e^{j\phi(X)}, \tag{15}$$

Therefore, if an estimate of the phase error can be made it is possible to correct the phase history data. First estimate, $\phi(X)$where $\phi_{est}(X) \approx \phi(X)$ then apply $e^{-j\phi_{est}(X)}$ to the corrupted range compressed image samples, $\tilde{G}(X, y)$. This is illustrated below

$$\tilde{G}(X, y)e^{-j\phi_{est}} = G(X, y)e^{j\phi_m}e^{-j\phi_{est}} = G(X, y)e^{j(\phi_m - \phi_{est})} \approx G(X, y).$$

If the phase error estimate is accurate then this will effectively cancel the phase error leaving the uncorrupted phase history data $G(X, y)$. Then taking a Fourier transform across the azimuth dimension will produce the corrected image. The following section will discuss the PGA algorithm which is used to estimate the phase error $\phi_{est}$ .

## Phase Gradient Autofocus

The PGA algorithm is composed of 4 main steps which include: circular center shifting, windowing, phase error estimation, and iteration. Figure 4 shows a flowchart of the PGA process with these steps, as well as other details necessary for proper implementation of the algorithm.

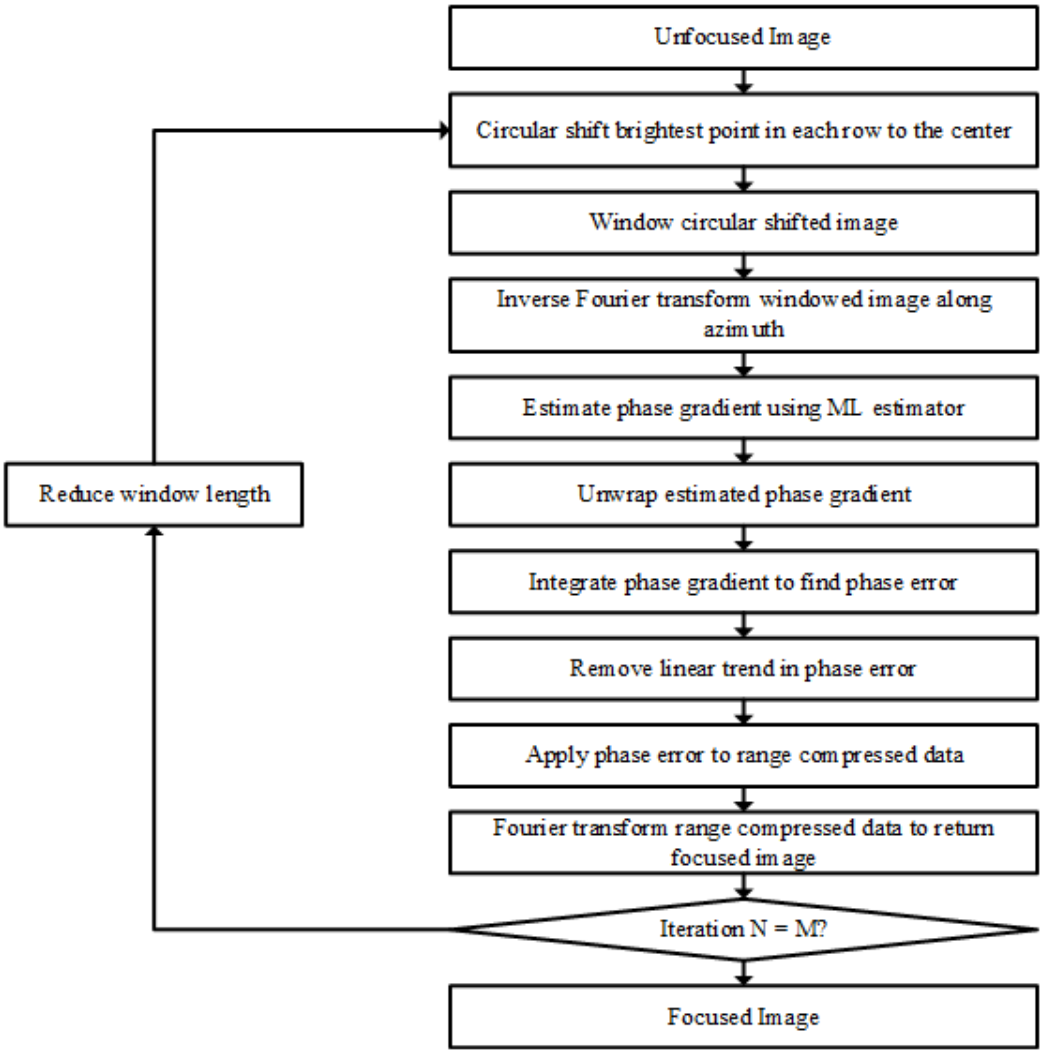


Figure 4: PGA Flowchart

*Center Shifting and Windowing*

In the image domain the brightest pixel in each range line is circular shifted to the center of the image. This aligns all the brightest points in a vertical line located on the middle azimuth column. Targets with strong returns compared to the clutter are more likely to provide an accurate phase error estimate than targets that have similar return power to that of the clutter.

Windowing in the image domain effectively raises the target-to-clutter ratio by removing some of the clutter while preserving the blurred impulse response of the brightest target on each range

line. Correctly calculating window length is important. If the window length is too small, part of the blurred impulse response of the center shifted target will not be included in the phase error calculation resulting in an inaccurate estimate. On the other had if the window is too large more noise is included in the estimate degrading the phase error estimate. There are numerous ways to choose the window length for the purpose of this paper the initial window length is chosen to be the entire image. The reason for this is explained in the following sections.

*Phase Error Estimation, Correction, and Iteration*

After the image is windowed the phase error is estimated using a maximum-likelihood (ML) estimate. This is done by finding the difference in phase between two adjacent columns in the phase history domain, which is the phase gradient between them. To accomplish this, a 1-dimensional inverse Fourier transform is applied to the azimuth dimension of the image to create phase history data. Then the ML phase gradient is estimated using the following equation:

$$\Delta\phi_{est}(X) = \angle \sum_{y=1}^{N} G^*(X,y)G(X-1,y), \tag{16}$$

where X is aperture position index in the frequency domain, y represents the range line, N is the number of range lines, $G$ is windowed and inverse Fourier transformed data, $G^*$ is the complex conjugate of $G$, and $\Delta\phi_{est}$ is the ML estimate of the phase gradient [1].

After the phase gradient is calculated it is bounded between $-\pi$ and $\pi$ and must be unwrapped in order to be useful. The unwrapped phase gradient is integrated and the linear trend is removed yielding the estimated phase error, $\phi_{est}$. Linear phase cause circular shifts in the image so it must be removed.

The negative of the phase error is then applied to the transformed data to correct the phase histories. A Fourier transform is applied across the azimuth dimension to take the phase history data back to the image domain.

The process starting with circular shifting and ending with the Fourier transform constitutes one iteration and is illustrated in Figure 4. After each iteration the window size is decreased. This occurs because each time the phase error estimate is applied; the image becomes progressively more focused causing the impulse response of each center shifted target to narrow.

The PGA used for this experiment uses 50 iterations and a large window length. This was done so that if there was a difference in performance by PGA for different image sizes it was not be due to the window length or because PGA failed to converge. The combination of a large window size and 50 iterations makes it possible to adjust the induced phase error and still have the PGA converge to the correct phase estimate. If the window was so small that some of the blurred pixels for a point target were not included within the window PGA would perform poorly because information needed to focus the point target is missing from the window. This scenario needs to be avoided in order to make conclusions about PGA's performance on different size images.

**Accuracy Metrics**

In order to determine the accuracy of the autofocus it is beneficial to analyze both the image itself to measure its focus and the phase error estimate to calculate its accuracy. Therefore, there were two methods used to measure the accuracy of PGA. A coherent change detection (CCD) image was formed from the original focused image and the refocused image after PGA to measure the image's focus. To measure the phase error estimate a mean absolute error (MAE) was calculated.

There is no single metric for determining whether an image is focused, nor is there a way to know if the phase error estimate made by PGA is accurate. In real world applications the phase error is

not known, therefore, it is impossible to know the true phase error exactly. In order to test if image size has an effect on PGA, an image was focused to remove the unknown phase error induced from the data collection. Then the focused image is blurred with a known quadratic phase so the estimated phase error from PGA can be compared to the applied phase error and an accuracy measure can be calculated. Mean absolute error was used to determine how well the estimate PGA found matched the applied phase error and CCD was used to compare the original focused image to the image after PGA processing. The next two sections will give an overview of MAE and CCD and clarify why they were used over other methods.

*Coherent Change Detection*

Coherent change detection makes it possible to not only measure how blurred the final focused image is by average coherence but also visualize the extent of the blurring. Normally CCD requires a registration of the two images first so the images align and a phase difference between them can be accurately calculated. For the purposes of this paper, however, registration is not necessary because the linear trend was removed from the applied phase error. Therefore no circular shift occurred and the images are aligned by default. That is, the geographical features in each image coincide to the same pixel locations in both images.

Once the images are aligned a cross correlation coefficient for local regions within the image is found using

$$\hat{a} = \left| \frac{\sum_{k=1}^{Z} f_k^* \, g_k}{\sqrt{\sum_{k=1}^{Z} |f_k|^2 \sum_{k=1}^{Z} |g_k|^2}} \right|, \tag{17}$$

where f is the original focused image, g is the image after PGA, and Z is the number of pixels in a local region. The cross correlation coefficient is for a local region and when done over regions across the entire image creates an interferometric image like one shown in Figure 5. The CCD shown in Figure 5 was made two data collections of the same patch of ground taken at different

time. The values for the cross correlation coefficient range from 0 when the images are completely different in the specified region and 1 where the images are the same. If the local region size, Z, is too small the cross correlation coefficient may not be accurate due to a lack of information. However, if the region is too big the resulting CCD image will have poor resolution [6]. The region sized picked for this paper was 25 because it was the smallest region size that did not create speckle in the resulting CCD image. An average of the cross correlation coefficients from every local region gives an average coherence which can be used to measure the blur of an image. The closer the average coherence is to 1 the closer the image after PGA is to the original which makes it possible to rate the performance of PGA.

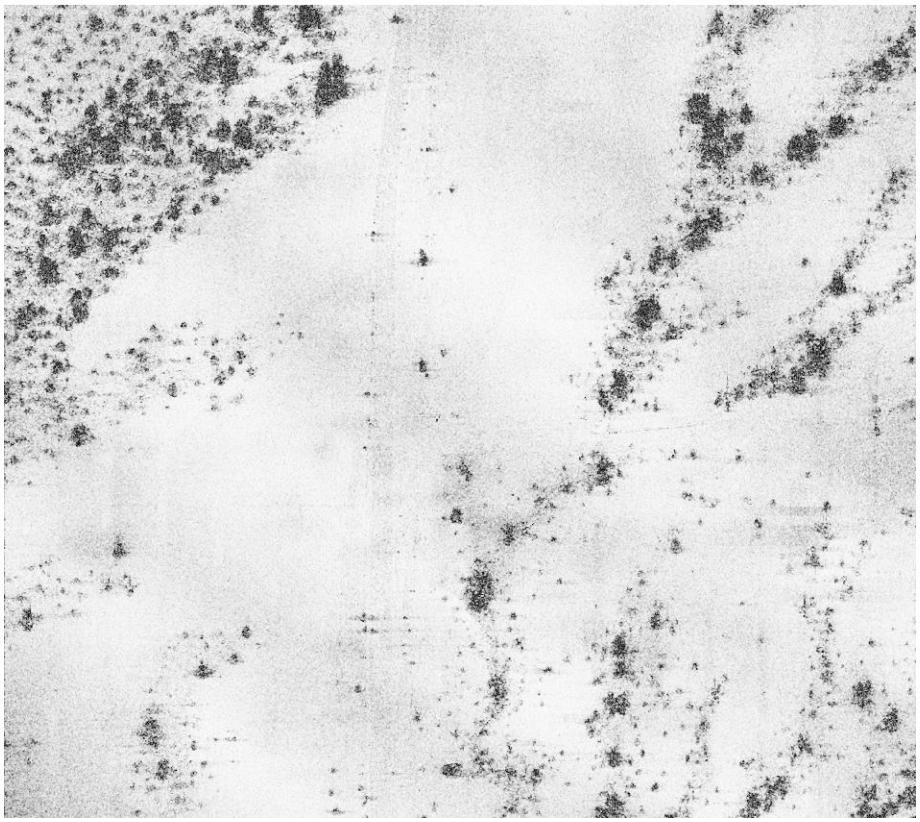

Figure 5: CCD created from two data collects

*Mean Absolute Error*

To measure the accuracy of the phase error estimate a focused image is blurred with a known phase error and statistics are used to compare the applied phase error to the estimated phase error. Mean absolute error (MAE) was used to evaluate the estimated phase error PGA found. MAE is given by

$$MAE = \frac{1}{M}\sum_{X=1}^{M}|\phi_{est}(X) - \phi(X)|, \tag{18}$$

where M is the number of azimuth bins. The MAE does a point-by-point comparison between the true phase error and the estimated phase error. MAE was chosen over Mean Squared Error (MSE) because MSE is heavily weighted by outliers. This could lead to the MSE being very large even when the general shape of the estimated phase error closely matches that of the applied phase error.

# CHAPTER IV

# EXPERIMENTS

The process used to find the minimum image size for PGA consists of 5 main steps: focusing a large image to remove any unknown phase error, inducing a known phase error, breaking the large image into smaller pieces, focusing those pieces individually, and comparing the results to a control case.

## Focus then Blur

First, the original large image is focused to remove any unknown error. After the image is focused it must be verified to have clearly defined point targets, that is, bright points must appear without any smearing. Any image where point targets remained blurred were not used for the rest of the experiment because the remaining unknown phase error was not negligible. Figure 6 and Figure 7 show examples of a focused SAR image and a blurred SAR image, respectively. Clear point targets can be seen at the center of Figure 6 and those same point targets appear smeared in Figure 7.

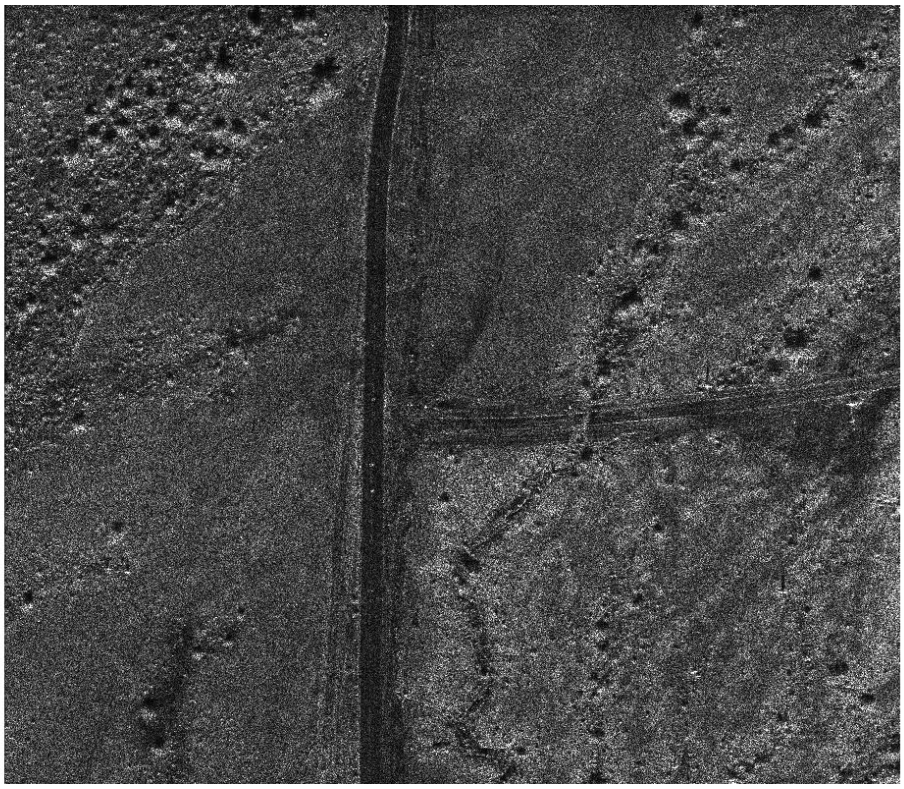

Figure 6: Example of Focused SAR Image

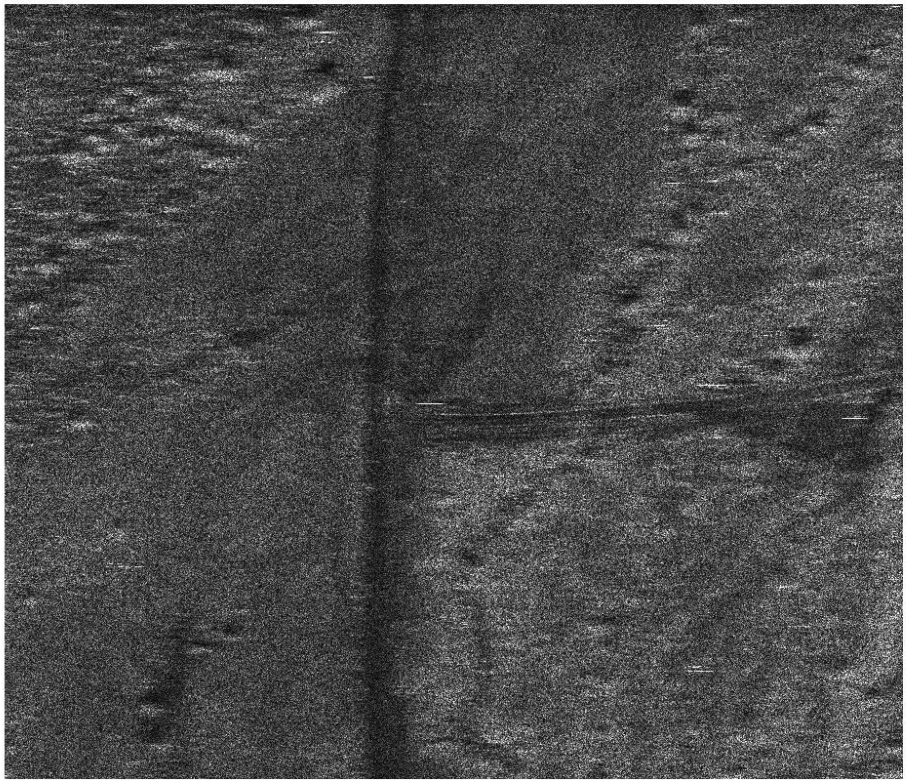

Figure 7: Example of Blurred SAR Image

Once the unknown phase error is removed a quadratic phase error is applied to the focused image, an example of a quadratic phase used is shown in Figure 8.

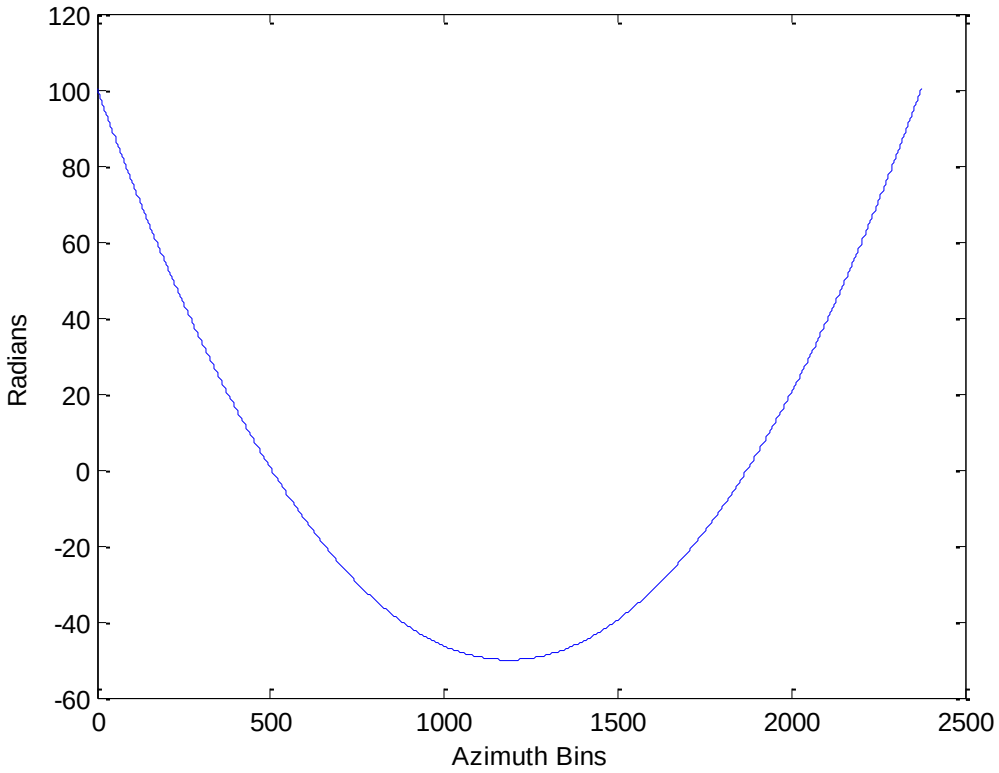


Figure 8: Quadratic Phase Error

The phase error, $\phi_{ap}(X)$, in Figure 8 is applied to every row in the range compressed image shown in Figure 9 by

$$\tilde{G}(X,y) = G(X,y)e^{j\phi_{ap}(X)}, \tag{19}$$

where $\tilde{G}(X,y)$ is the blurred range compressed image and $G(X,y)$ is the focused range compressed image. After performing a Fourier transform across azimuth on the blurred range compressed image, shown in Figure 9, the result is the blurred image shown in Figure 10.

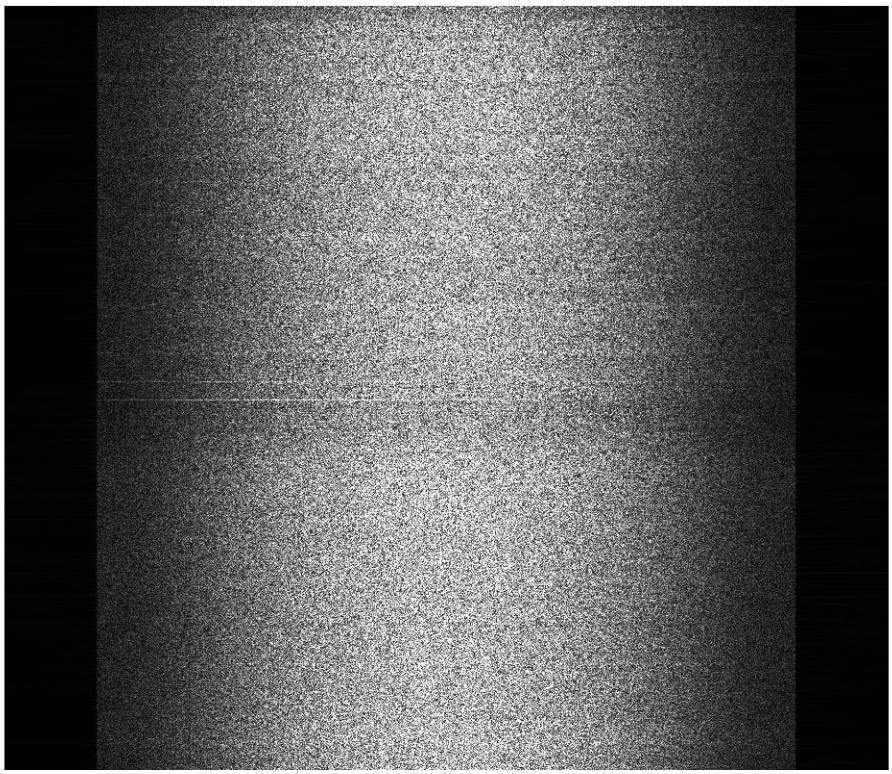

Figure 9: Range compressed image before azimuthal compression

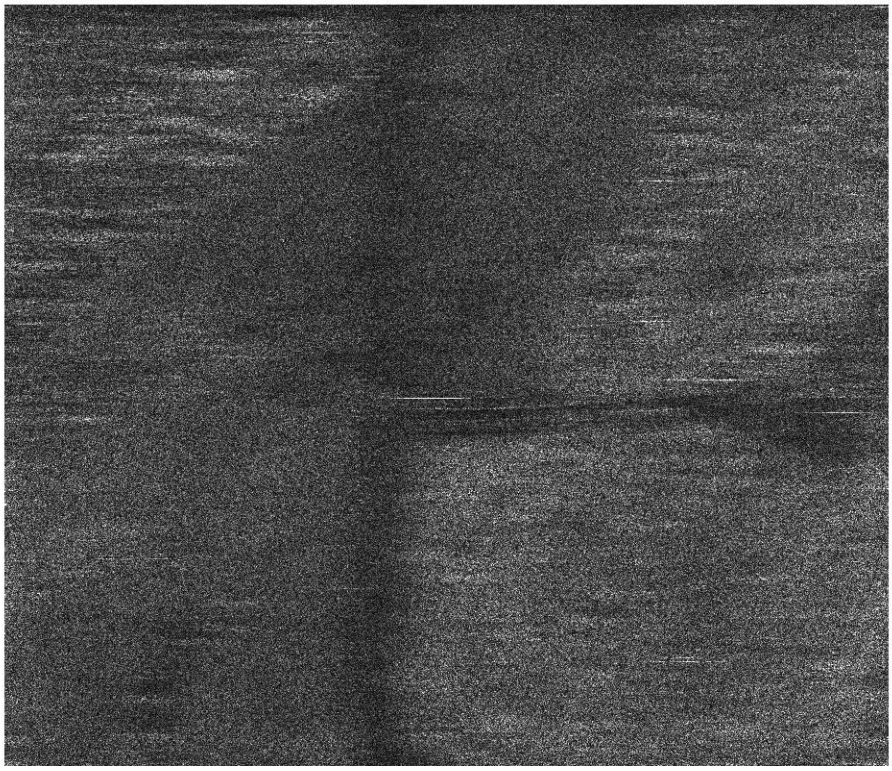

Figure 10: Image blurred with known phase error

The range compressed image shown in Figure 9 is a range vs. azimuthal frequency image. There is a Taylor weighting across azimuth to control the side lob levels of the impulse response. The range compressed image is also zero padded to reduce aliasing effects and make the image formed after performing a Fourier transform along azimuth more visually pleasing.

*Quadratic Phase Error*

There are some key aspects about the phase error in Figure 8 that need to be addressed. Notice that the quadratic phase error does not have a linear component. Phase errors with linear trends cause circular shifts to occur in the image and PGA is not capable of detecting linear phase error. Which means, if there was a linear component in the applied phase error a circular shift would be present in the refocused image after PGA and registration would become necessary in order to do a CCD. However, without a linear component in the applied phase error no registration is required and the CCD can be calculated as discussed in chapter III.

Finally, a quadratic phase error was used due to its predictable blurring effect on the image. Figure 11 a) shows a single focused artificial point target and b) – d) show how increasing the amplitude of the quadratic produces a larger blur footprint. This property of the quadratic phase error makes it possible to control the amount of blurring which will be necessary for testing PGA's performance for different sized images.

a)

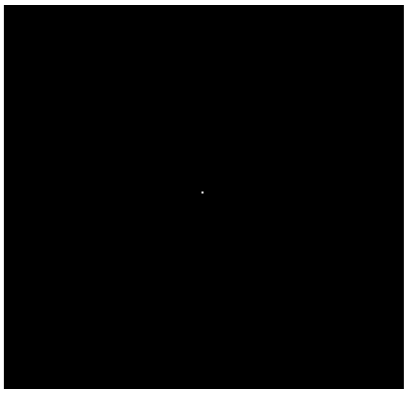

b)

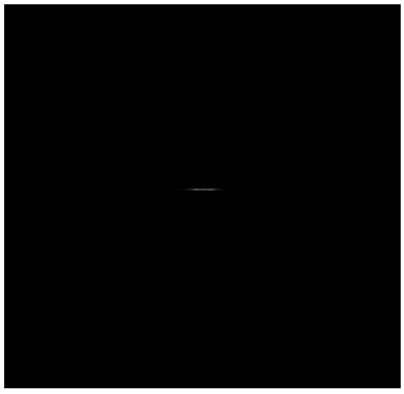

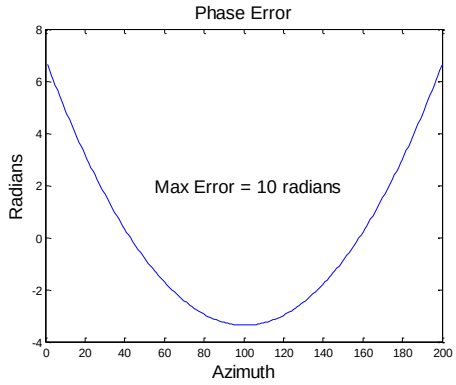


c)

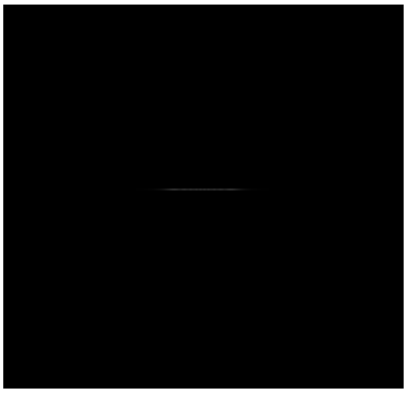

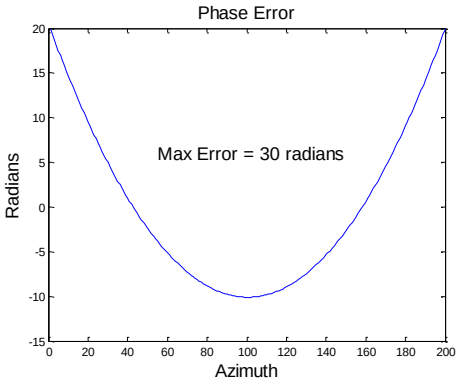


d)

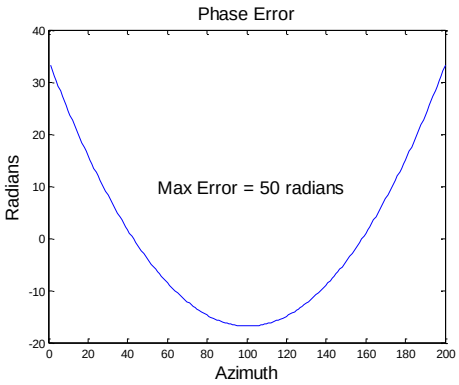


Figure 11: Point Target with Various Degrees of Blur

### Experiment 1: Consistent Phase Error

The first experiment's goal was to evaluate PGA's performance when the only parameter that varies is the size of pieces into which the image is broken. Therefore, no matter what size pieces the image is to be broken into the phase error is consistent.

The image was broken into 6 piece sizes for evaluation. The piece sizes were chosen by dividing the length and width of image in half 5 times. The resulting image piece size are approximately

- 2600 x 3000 (the entire image),
- 1300 x 1500 (4 total pieces),
- 650 x 750 (16 total pieces),
- 325 x 375 (64 total pieces),
- 160 x 190 (256 total pieces), and
- 80 x 90 (1024 total pieces).

There were 3 phase error amplitudes tested in this experiment: 10 radians, 100 radians, and 350 radians.

After the focused image is blurred with the quadratic it is broken into pieces and each piece is focused individually. The focused pieces are recombined to form a refocused image. Then a CCD is calculated using the original focused image and the refocused image. Results of the CCD and the estimate PGA found for all image piece sizes of a patch blurred with a 10 radian maximum error are shown in Figure 12 - Figure *23*.

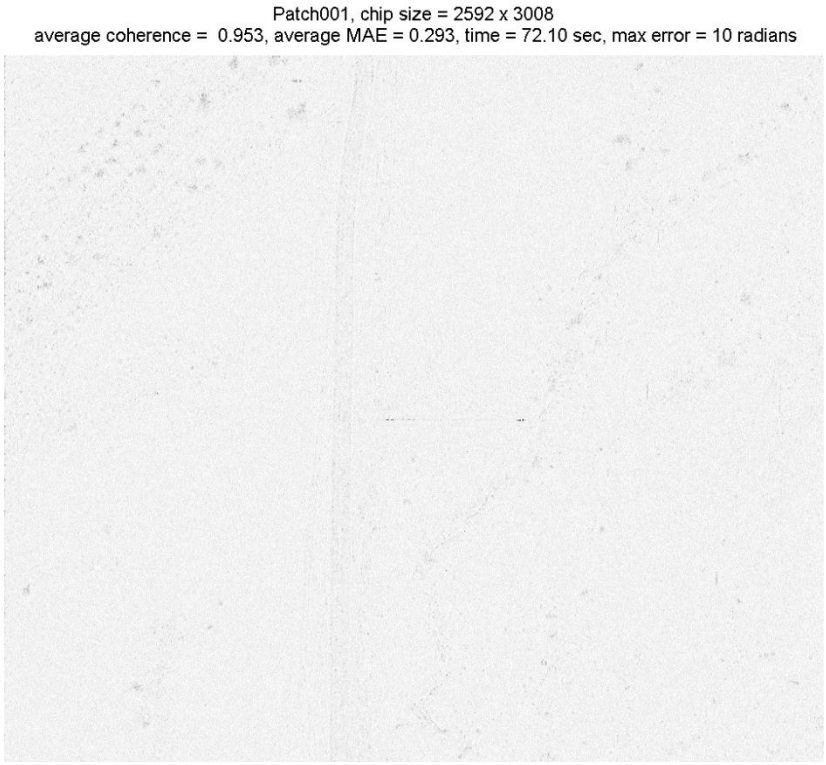


Figure 12: CCD after entire image focus

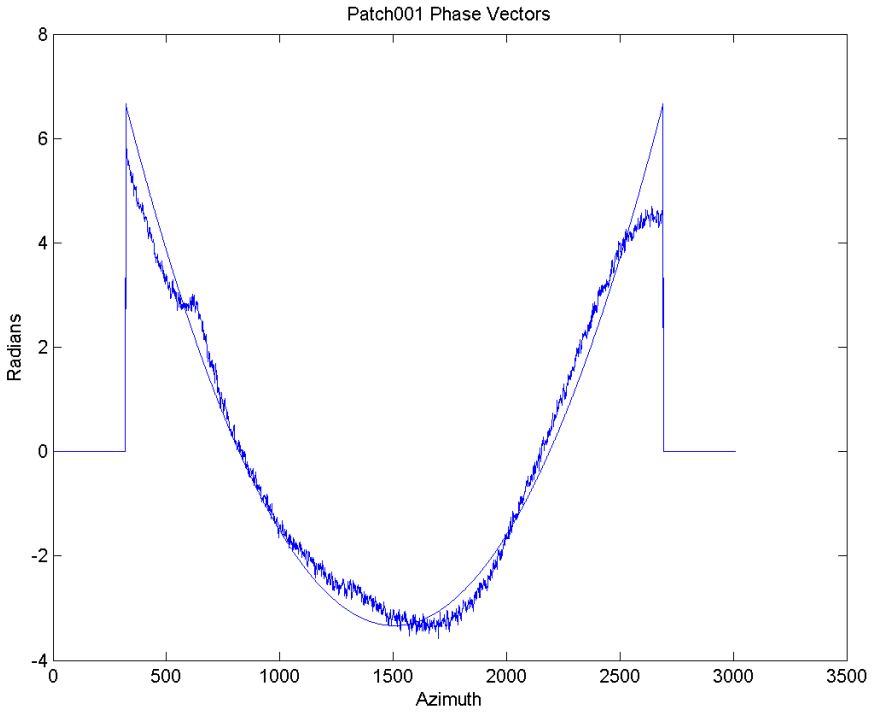


Figure 13: Applied and estimated phase error for entire image focus

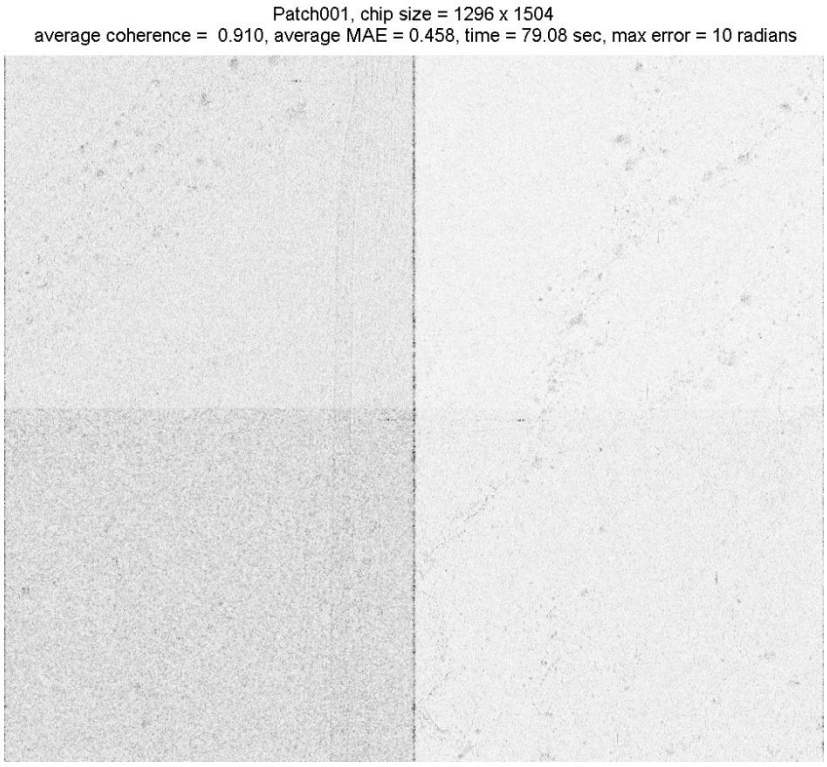


Figure 14: CCD after 1/2 by 1/2 image focus

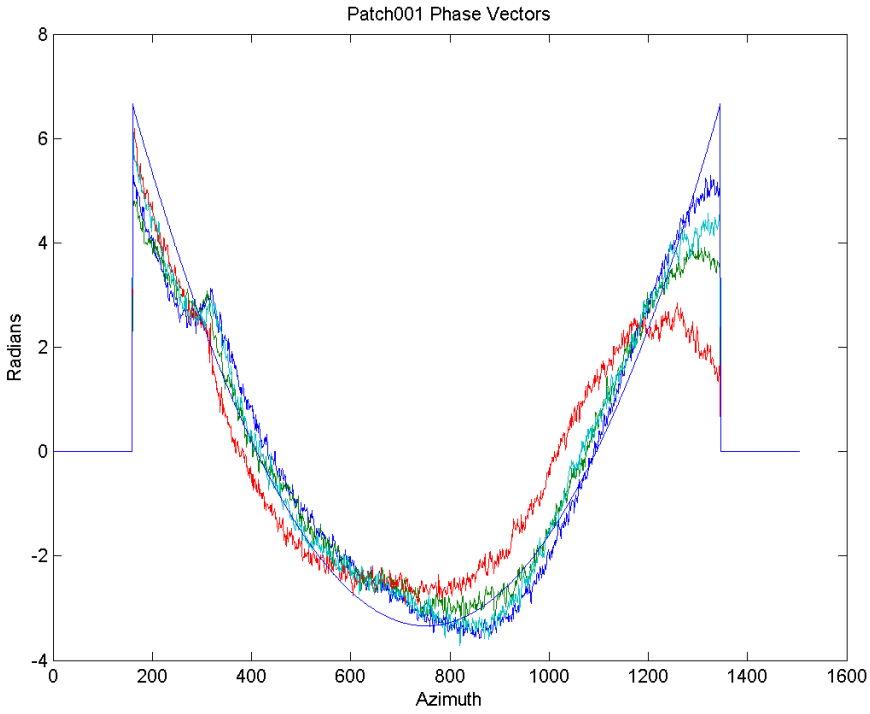


Figure 15: Applied and estimated phase errors for the 4 pieces

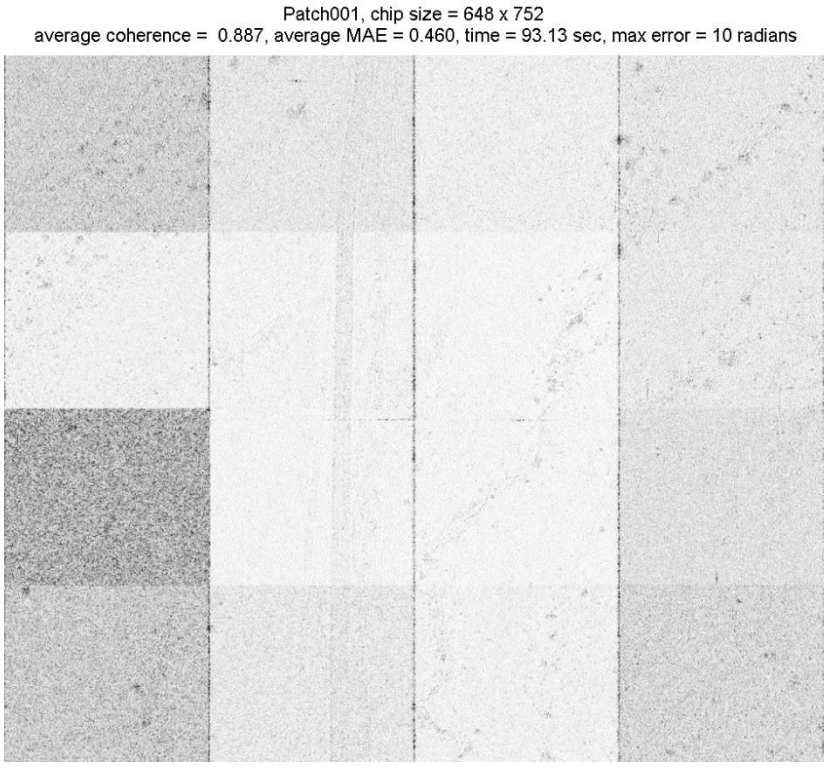


Figure 16: CCD after 1/4 by 1/4 image focus

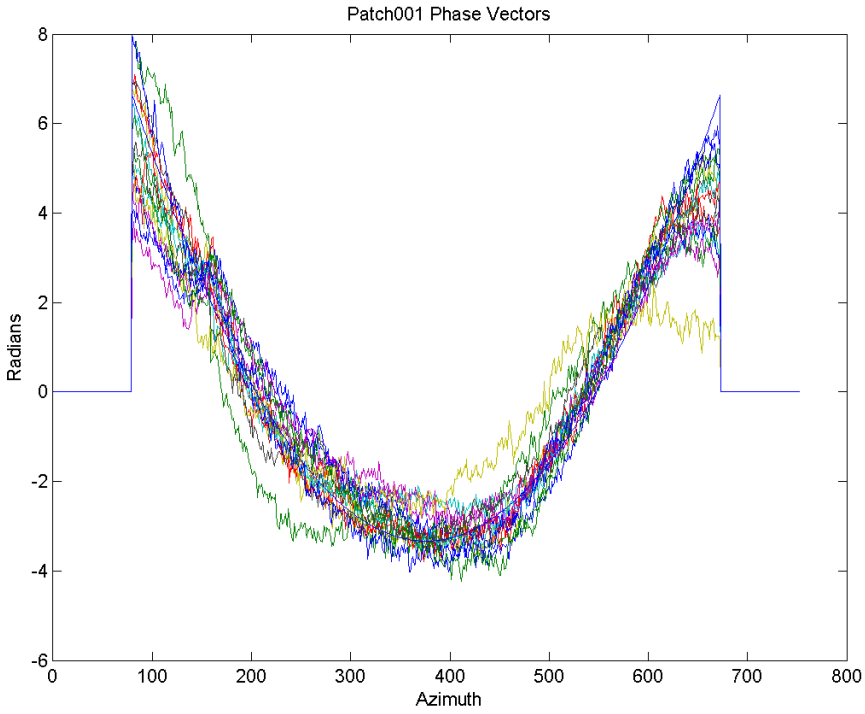


Figure 17: Applied and estimated phase errors for the 16 pieces

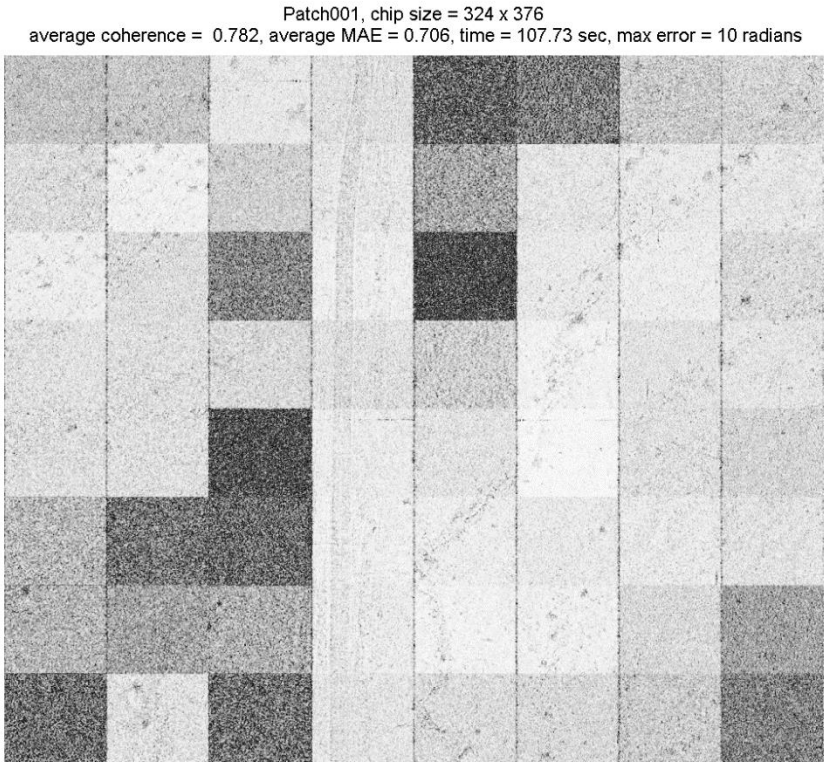


Figure 18: CCD after 1/8 by 1/8 image focus

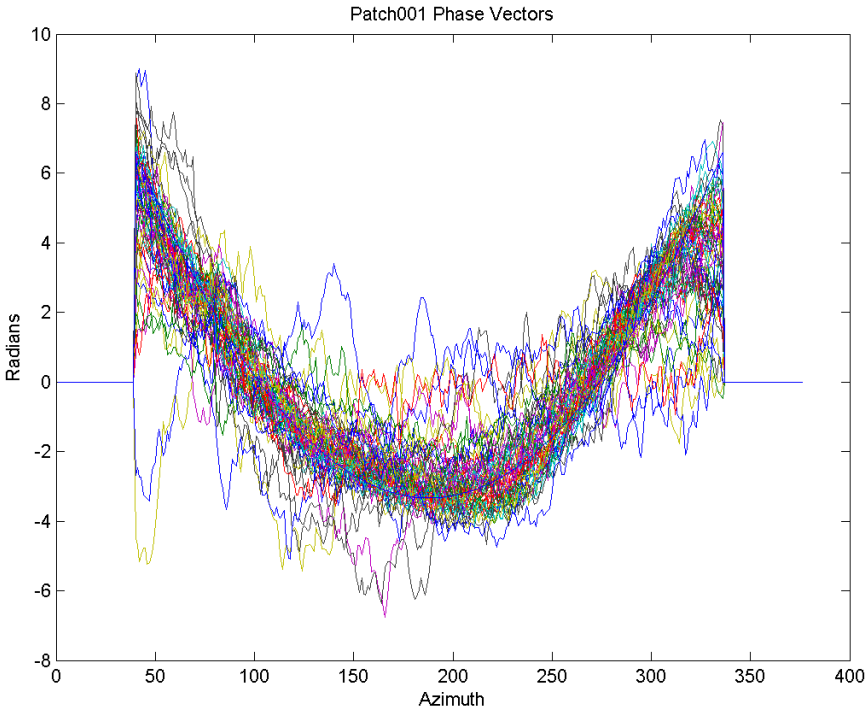


Figure 19: Applied and estimated phase errors for the 64 pieces

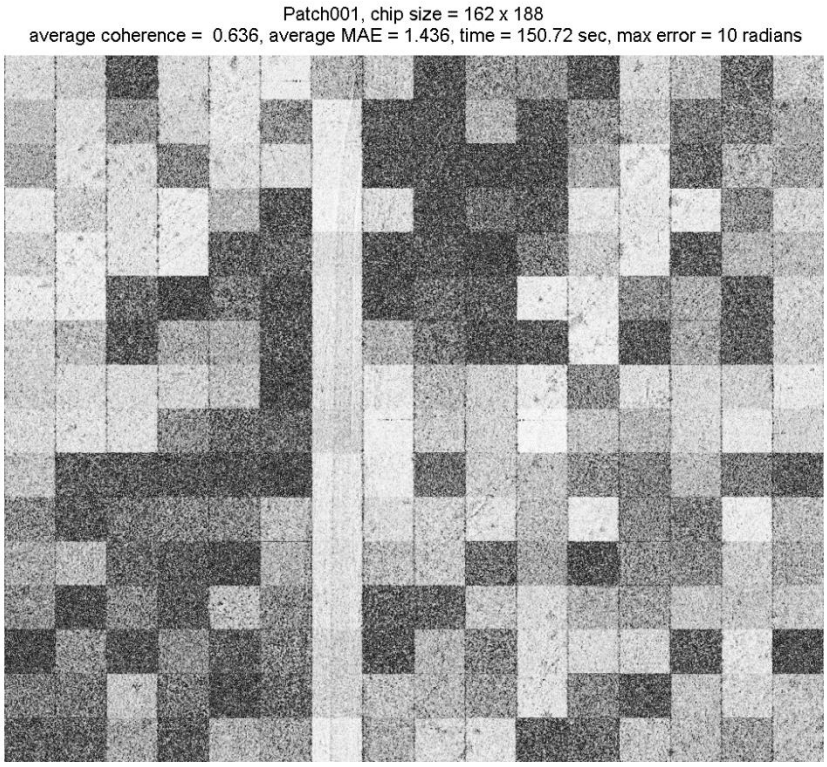


Figure 20: CCD after 1/16 by 1/16 image focus

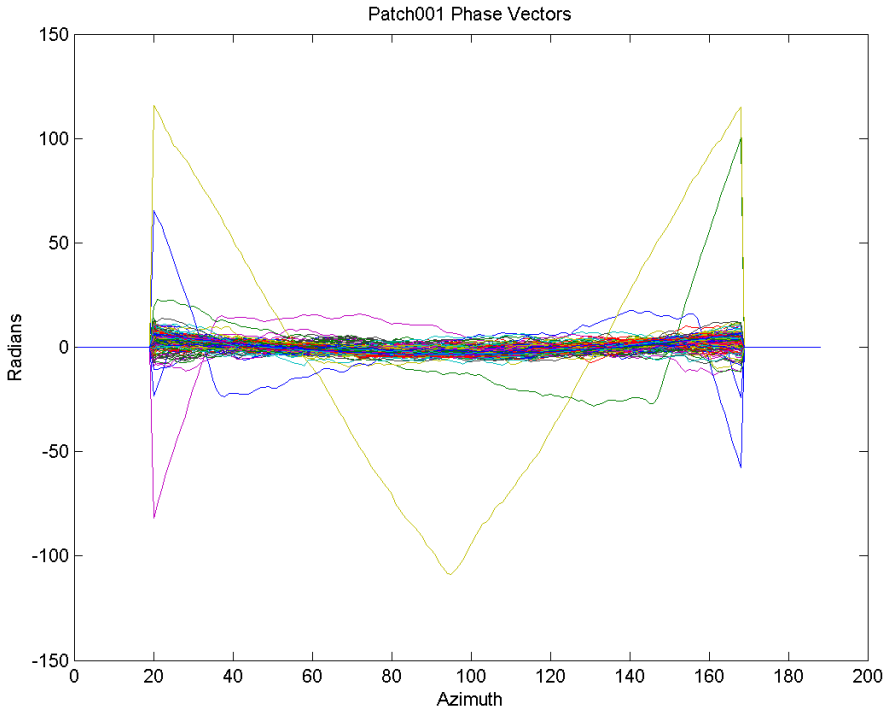


Figure 21: Applied and estimated phase errors for the 256 pieces

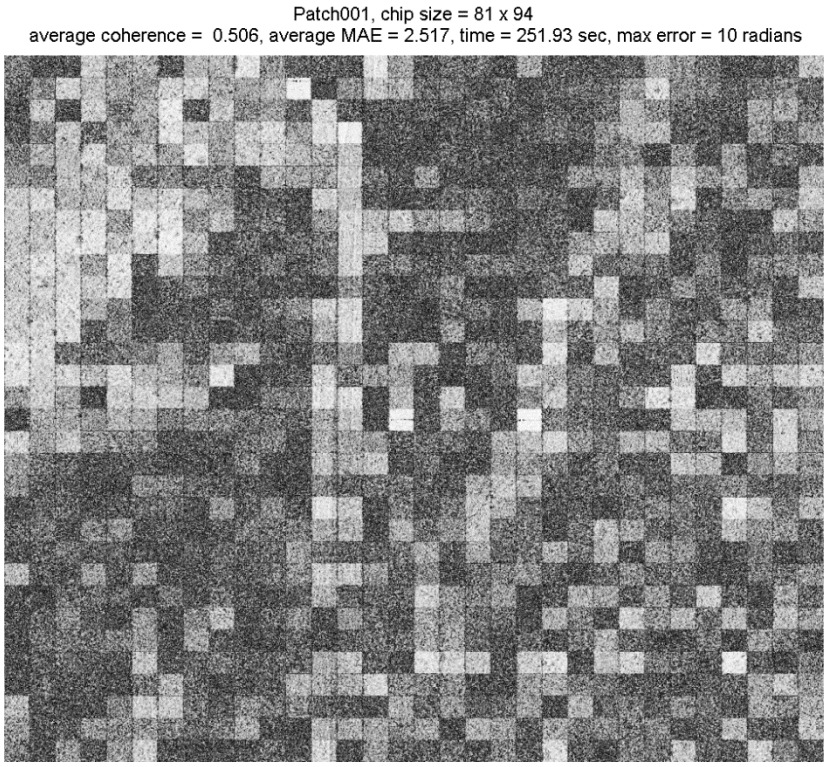


Figure 22: CCD after 1/32 by 1/32 image focus

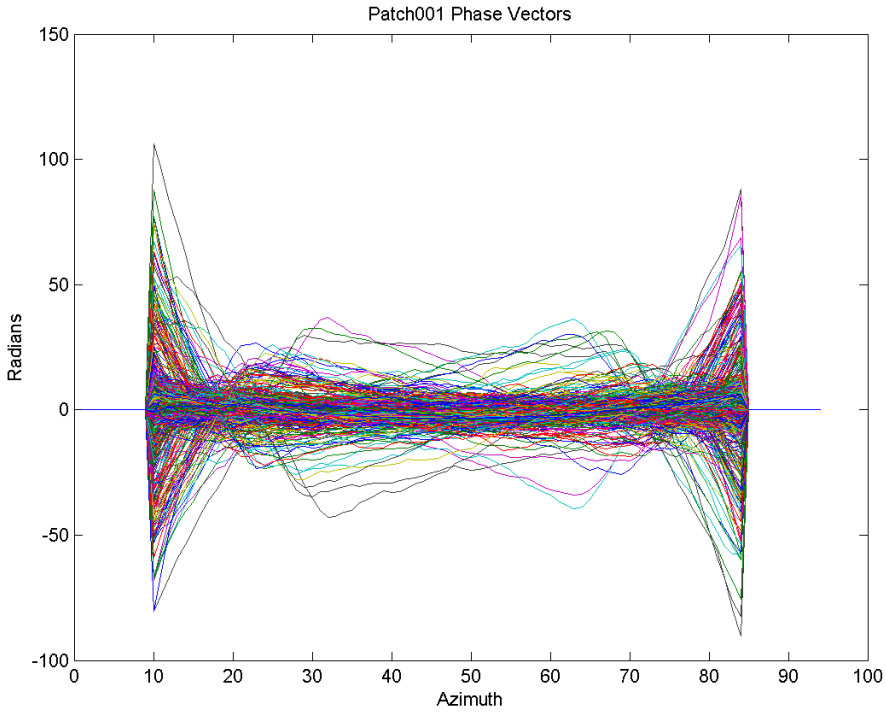


Figure 23: Applied and estimated phase errors for the 1024 pieces

*Experiment 1 Results*

The image shown in the CCD images above has variety of characteristics each of which have an effect on PGA's performance. The top left corner of the image has the most structure. There are shrubs and rocks that create a combination of bright and shaded areas. As the image piece sizes decrease this structure seems to help PGA find a more accurate phase error estimate. This is shown in Figure *18*, Figure *20*, and Figure *22* where the pieces that perform the best are mainly the ones containing this type of structure. Also, a road runs down the middle of the image with a vertical line of strong returns that accompanies the road. Figure *18* and Figure *20* best illustrate this by the column of high coherence along the center of the image where the road is located. Regions where the PGA does the worst are where there is little to no structure accompanied with low power returns. Figure *18* and Figure *20* show areas of low coherence on each side of the road where the clutter appears uniform and from Figure *6* those regions are also darker than the surrounding area.

The following data were collected from six complex SAR images. Figure 24 shows for a phase error of 10 radians the coherence decreases as the image piece decreases. Figure 25 shows the MAE increases as the image piece size decreases which means the reason for the loss of coherence is PGA being unable to calculate the correct phase error. This result is not entirely surprising because PGA is a maximum likelihood estimator, therefore, the more information PGA has to use the more accurate the estimate. PGA's performance was significantly worse for the smallest two image piece sizes for every image tested even with a relatively small phase error of 10 radians.

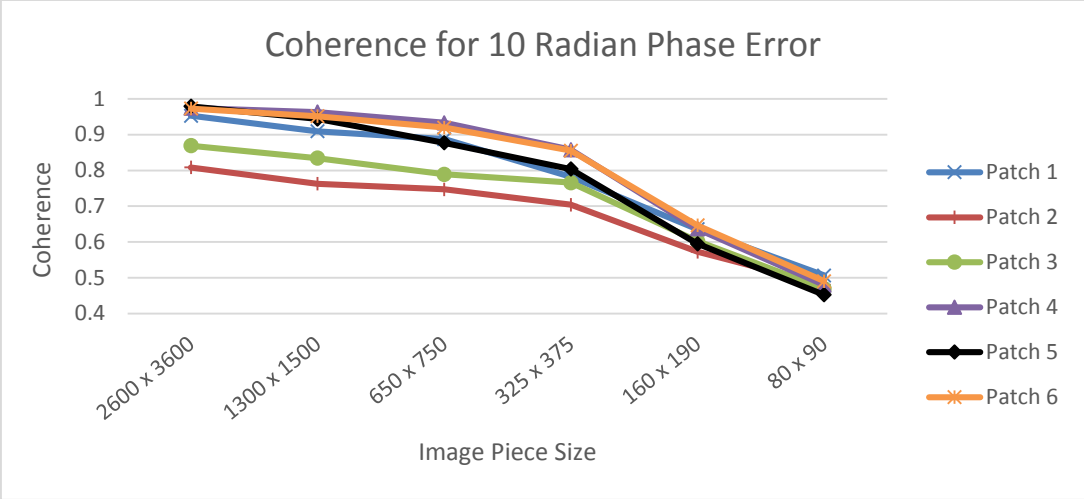


Figure 24: Coherence when 10 radian phase error is applied

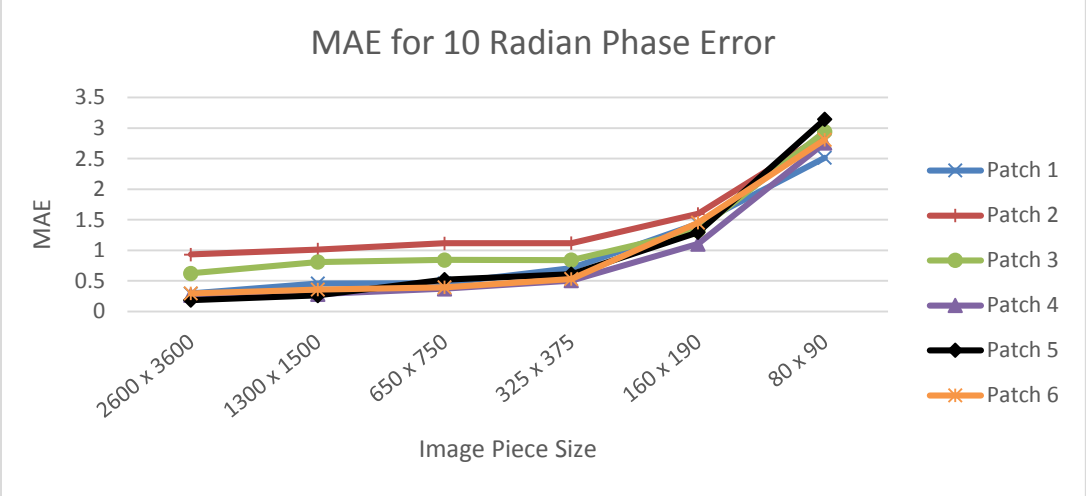


Figure 25: MAE when 10 radian phase error applied

A similar trend is seen when the phase error amplitude is increased to 100 radians. Figure 26 shows there is now a sharp decline in coherence for the third smallest piece size along with the two smallest image piece sizes. The three largest image piece sizes all appear nearly unaffected by the larger phase error. Figure 27 shows an increase in MAE for the image piece sizes that saw a decrease in coherence. The 100 radian phase error caused a much larger MAE for the two

smallest image piece sizes than the 10 radian phase error did but the coherence did not drastically decrease.

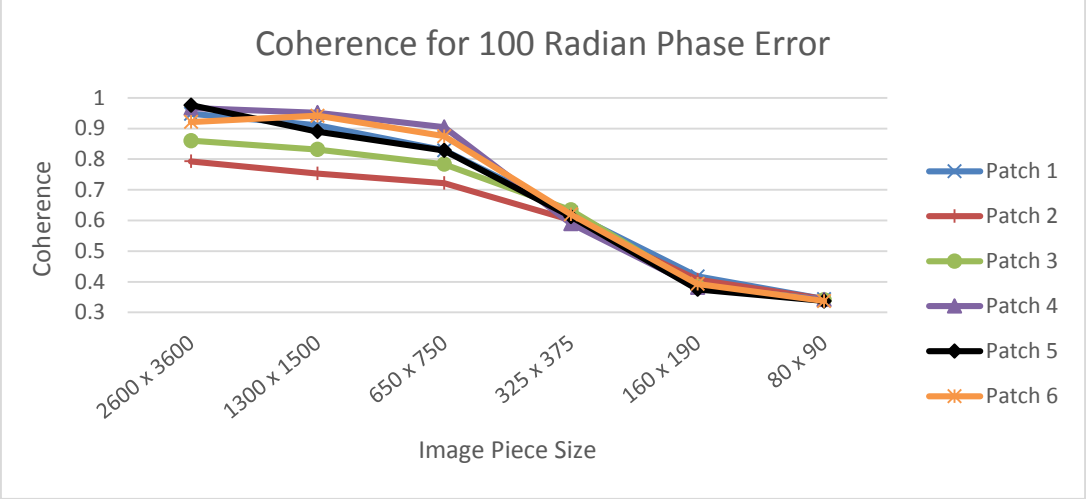


Figure 26: Coherence when 10 radian phase error is applied

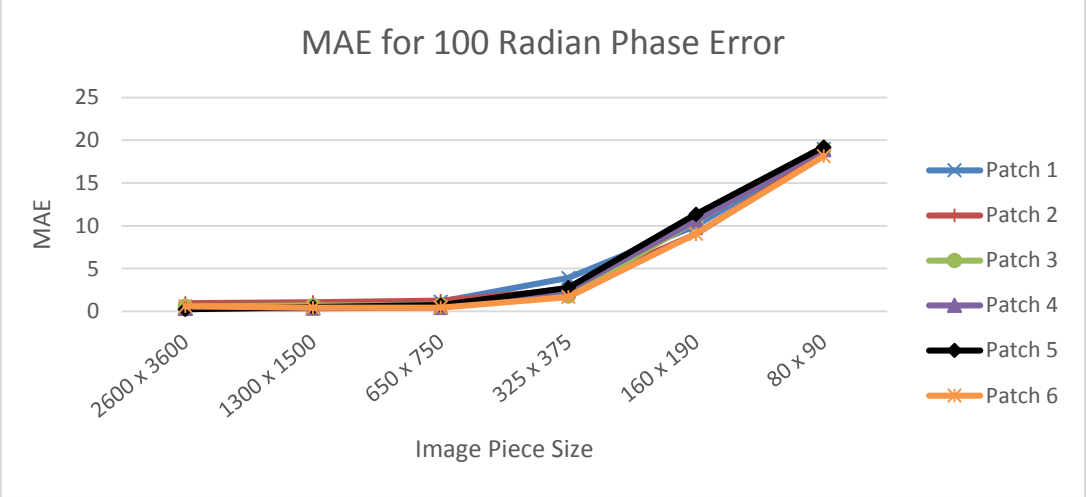


Figure 27: MAE when 10 radian phase error applied

The largest phase error tested in this experiment was 350 radians. All image piece sizes saw a decrease in coherence when a phase error of 350 radians was applied compared to the smaller phase errors. However, the entire image focus saw a minimal decrease.

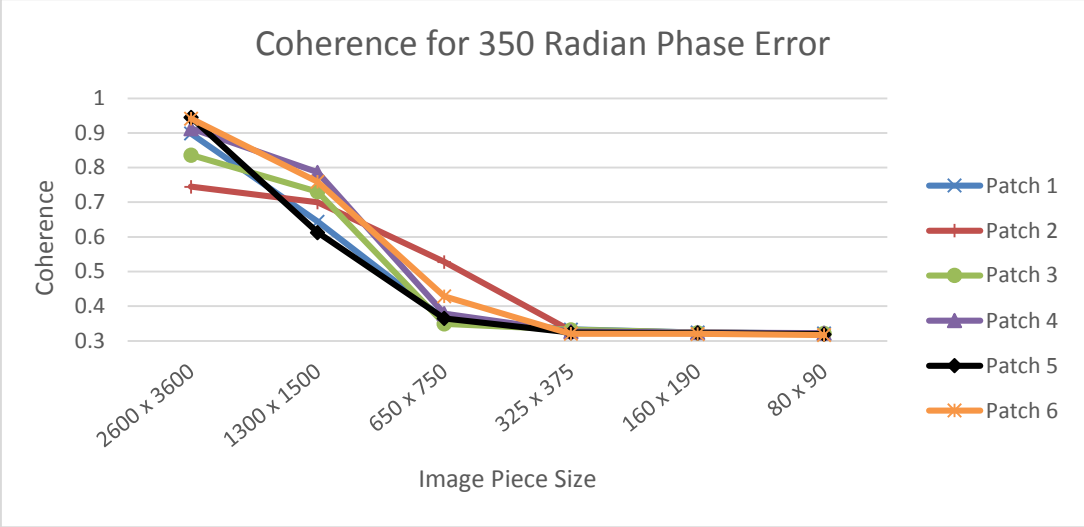


Figure 28: Coherence when 10 radian phase error is applied

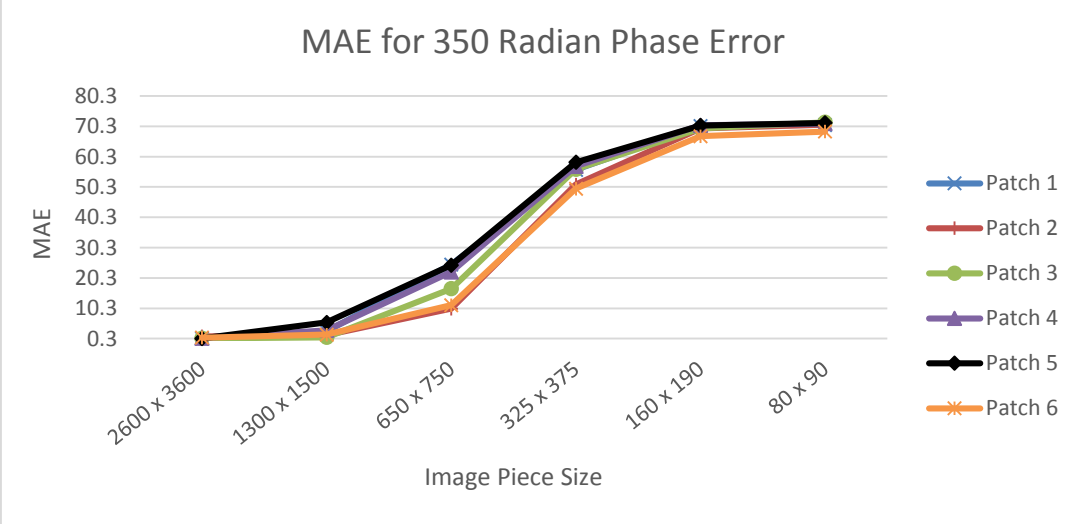


Figure 29: MAE when 10 radian phase error applied

### Experiment 2: Exponentially Decreasing Phase Error

A second experiment was needed to test whether the smaller image piece sizes were failing to focus due to their smaller image size or because the phase error was too large for that size image. Therefore, for the second test the amplitude of the quadratic used decreased with the size of pieces into which the image was broken. This was done because a small piece of the image would not be able to correct for a phase error that causes a blur footprint larger than the piece itself. For example, if the pieces of the image were 200x200 pixels and the blur footprint caused by the applied phase error was larger than 200 pixels, all the information needed to properly estimate the phase error would not be within one piece of the image. Therefore, PGA would find an incorrect phase error. For this reason the quadratic applied decreases in amplitude along with the size of the image pieces.

In order to decrease the phase error as the image piece size decreases the total range of the quadratic phase error applied was set to be a percentage of the azimuth dimension of the image pieces. For example if the amplitude of the phase error was 10%, for a 200x200 pixel image piece, the quadratic would have a maximum error of 20 radians. Similarly, for a 1000x1000 pixel image the quadratic would have a maximum error of 100 radians. By defining the maximum error of the quadratic as a percent of the image piece size it insures the blur footprint will not exceed one image piece's dimensions without exceeding them all.

The same image piece sizes used in the previous experiment were used in for this one. The image pieces were evaluated with the application of 3 phase error percentages 5%, 15%, and 25%.

Once the large image is blurred with the quadratic phase error it is divided into pieces and each piece is focused individually. All pieces are recombined to form a refocused image and a CCD is calculated using the original focused image and the recombined refocused image. Results from

the same image tested in the first experiment with a 5% phase error per piece are shown in Figure 30 - Figure 35.

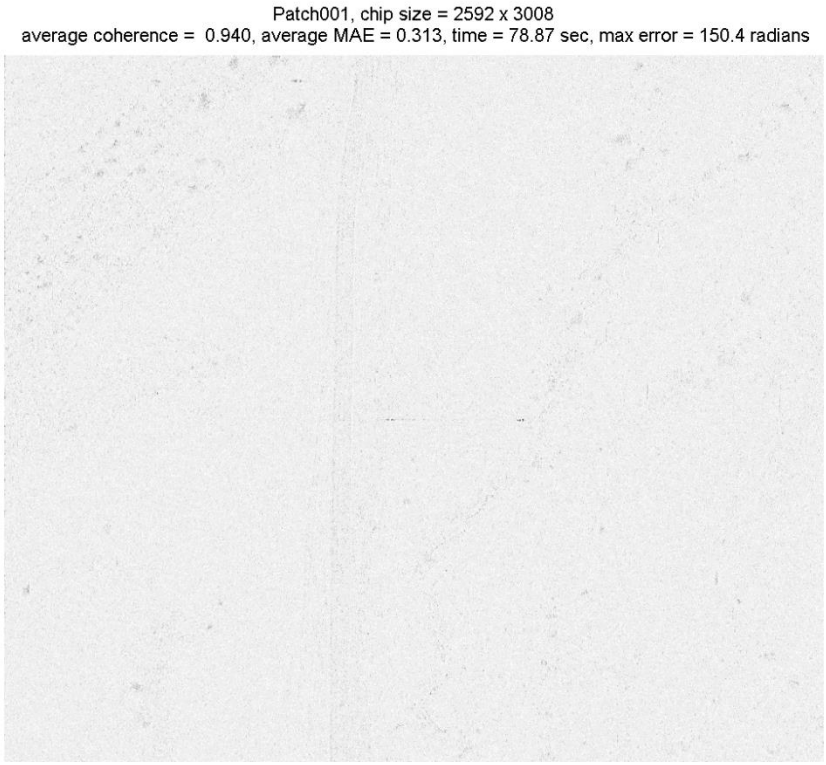


Figure 30: CCD after entire image focus

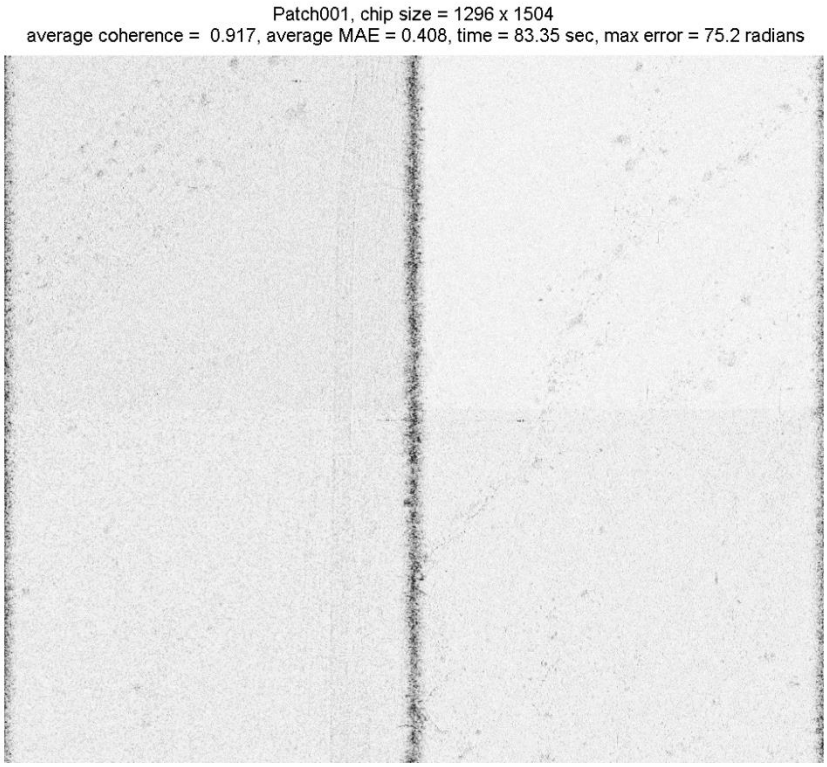


Figure 31: CCD after 1/2 by 1/2 image focus

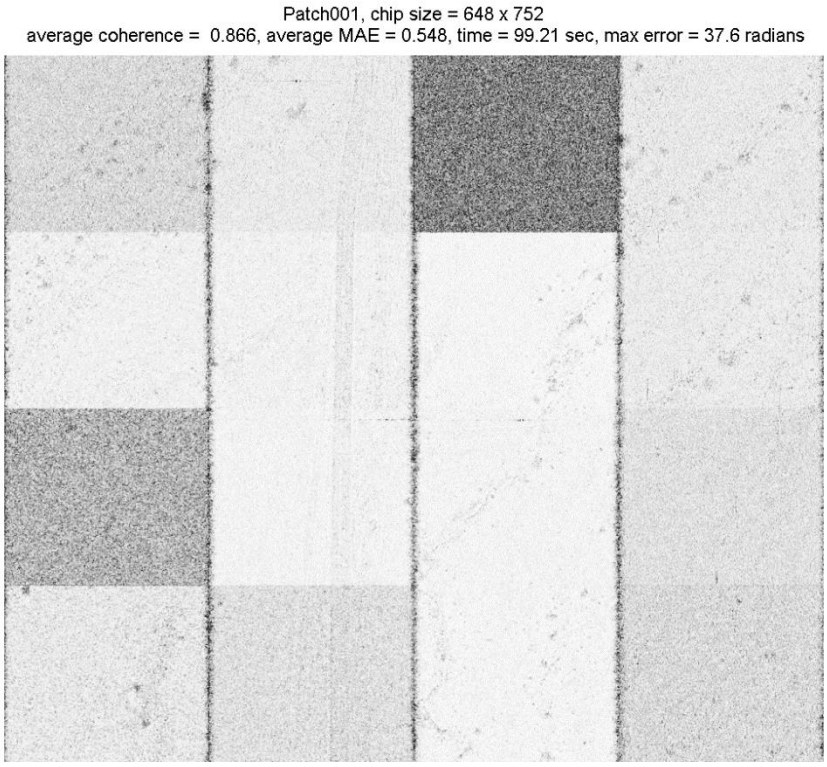


Figure 32: CCD after 1/4 by 1/4 image focus

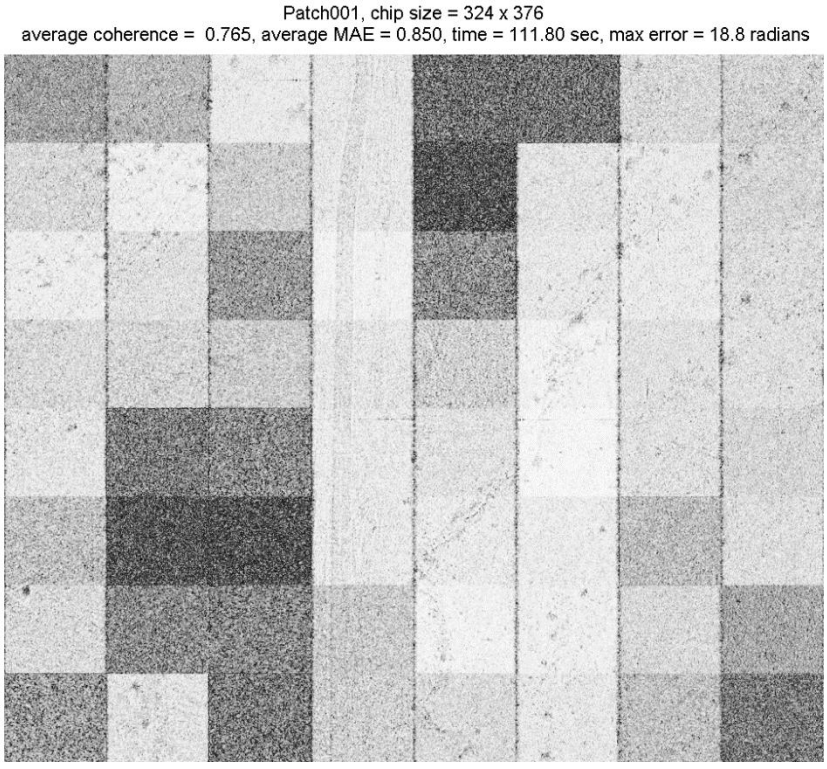


Figure 33: CCD after 1/8 by 1/8 image focus

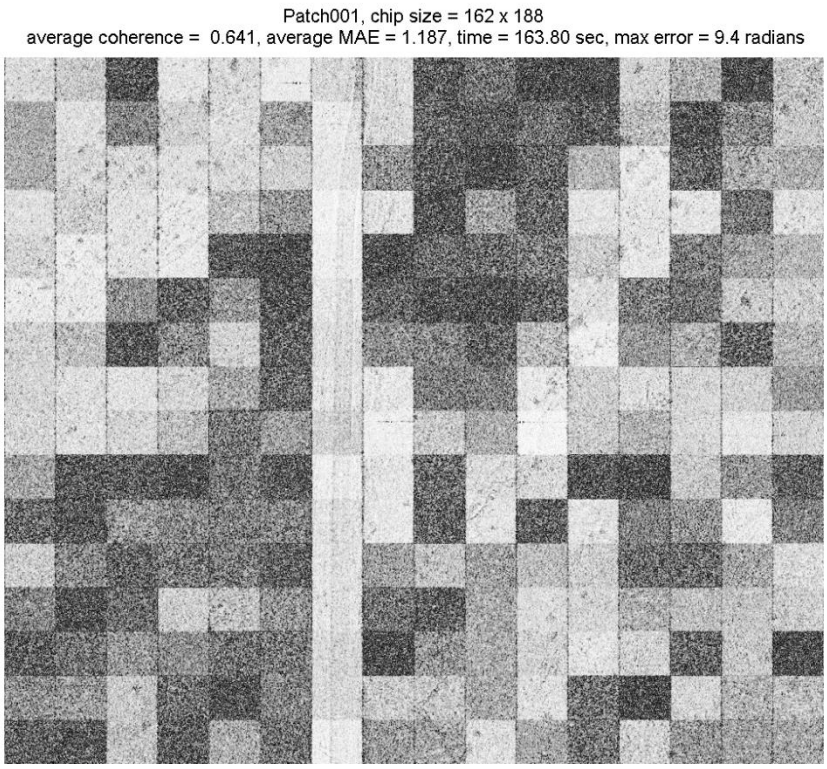


Figure 34: CCD after 1/16 by 1/16 image focus

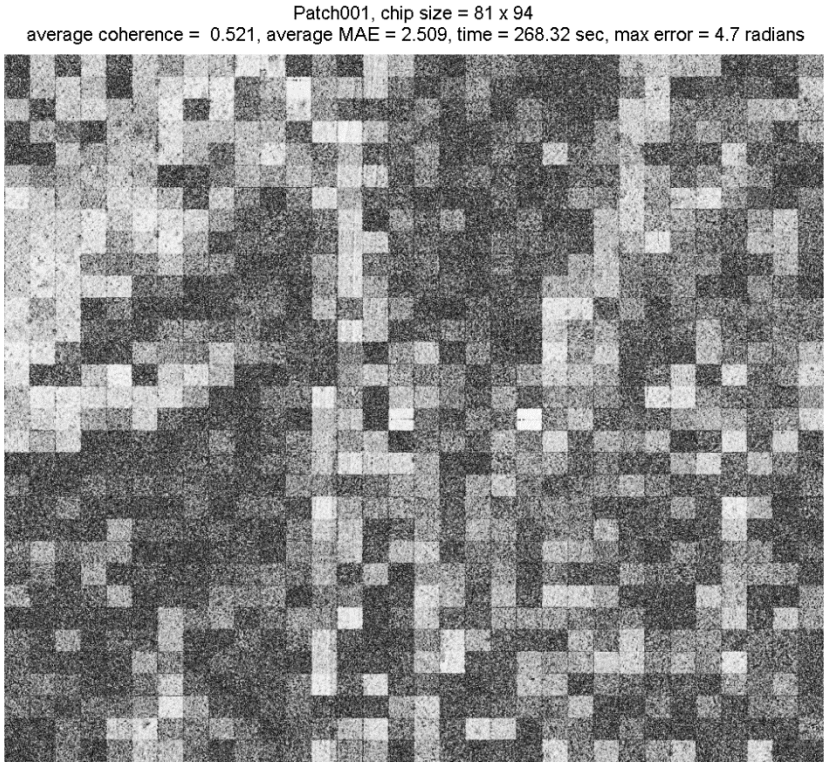


Figure 35: CCD after 1/32 by 1/32 image focus

*Vertical Lines*

Vertical lines of incoherence appear at the intersection of any two images pieces. This is because when the image is divided, points that are blurred across the boundary of two image pieces will be missing information. The missing information makes it impossible for PGA to focus those points even if the phase error was known exactly. This also means that the width of the vertical lines is dependent on the size of the phase error. Illustrated by Figure 31, which has a maximum phase error of 75.2 radians and a wide vertical line down the center of the image, and Figure 35 which has a maximum phase error of 4.7 radians and nearly invisible vertical lines.

*Experiment 2 Results*

The CCD images for the second experiment are similar to the first experiment except Figure *32* has an image piece fail to focus in a region of the image where there is little structure and low power returns. The image in Figure *32* was blurred with a quadratic with a range of 36 radians over 3 times larger than the phase error applied in the first experiment. PGA was not able to focus the larger phase error in that region because of a lack of strong point targets with the correct phase error. An image can fail to focus because of a lack of strong targets so the phase error cannot be distinguished from the clutter but also from strong targets that have a different phase error than the rest of the image. Most of the time a strong target with incorrect phase error is not a problem because there are enough other targets to compensate, however, as the image size decreases the strong incorrect point target can dominate.

The following data were collected from 6 complex SAR images. Figure 36 shows a plot of the coherence and Figure 37 shows the mean absolute error when a 5% phase error was applied to each of the image piece sizes. The exact phase error amplitude applied to each image is shown in Figure 38. The graph of coherence in Figure 36 suggests, for a small phase error relative to the image piece size (only 5%), that coherence tends to decrease as the image size decreases. Figure 37 shows an increase in MAE as the image size decreases implying that PGA is less accurate

when applied to a smaller image. This supports the evidence from experiment 1 that smaller image size leads to a worse phase error estimate from PGA.

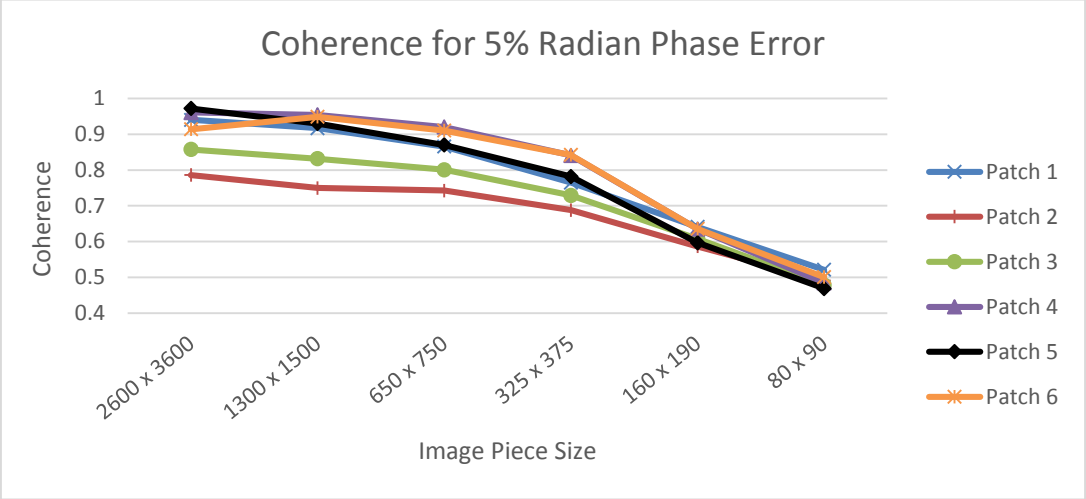


Figure 36: Normalize coherence when a 5% error is applied

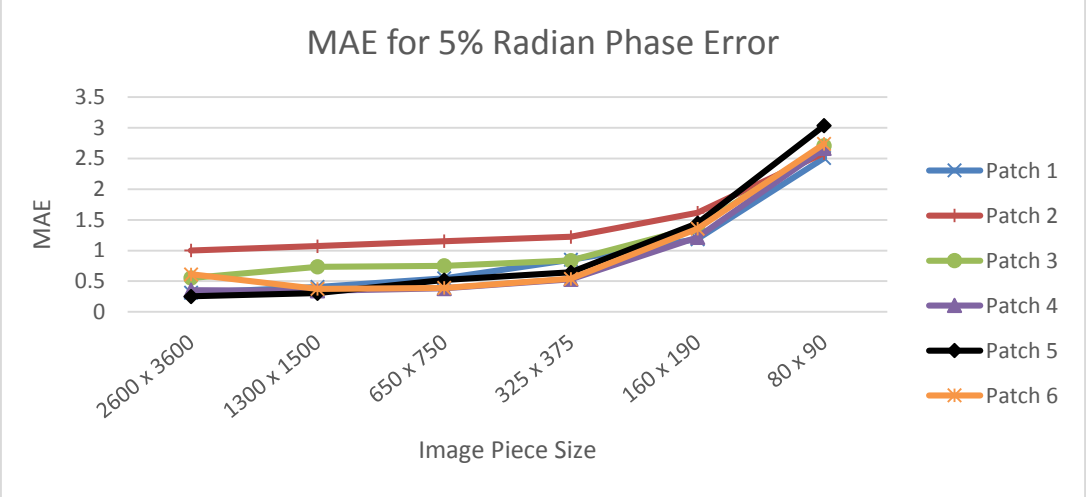


Figure 37: MAE when a 5% error is applied

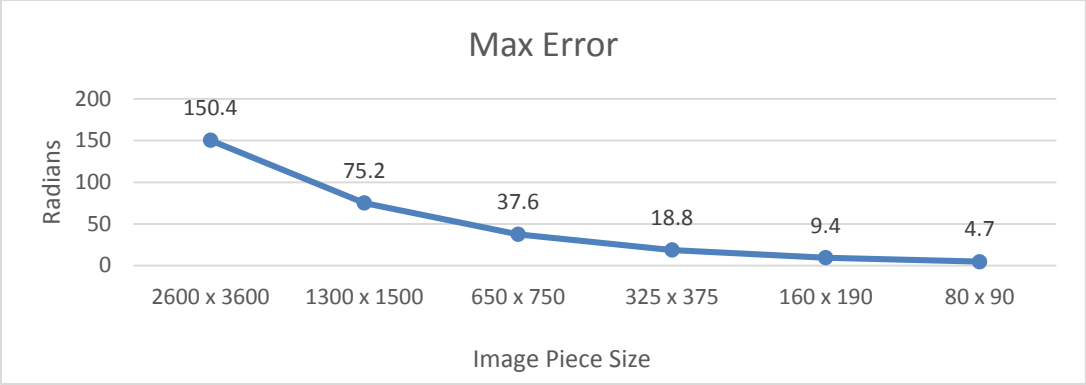


Figure 38: Maximum error applied to each image

The coherence for the largest 3 image piece sizes is nearly constant from the 5% phase error to the 15% phase error. Even in cases of very large phase errors (450 radians in one case), a significant drop in coherence was not seen. This means larger images can correct much larger phase errors. The phase error applied to the entire image was over 450 radians and PGA did a far better job estimating it than for the smallest image size with only a 14 radian phase error.

The third smallest image piece size saw a decrease in coherence for the 15% phase error compared to the 5% case. This suggests that as the error increases smaller image sizes have a harder time calculating the correct phase error estimate.

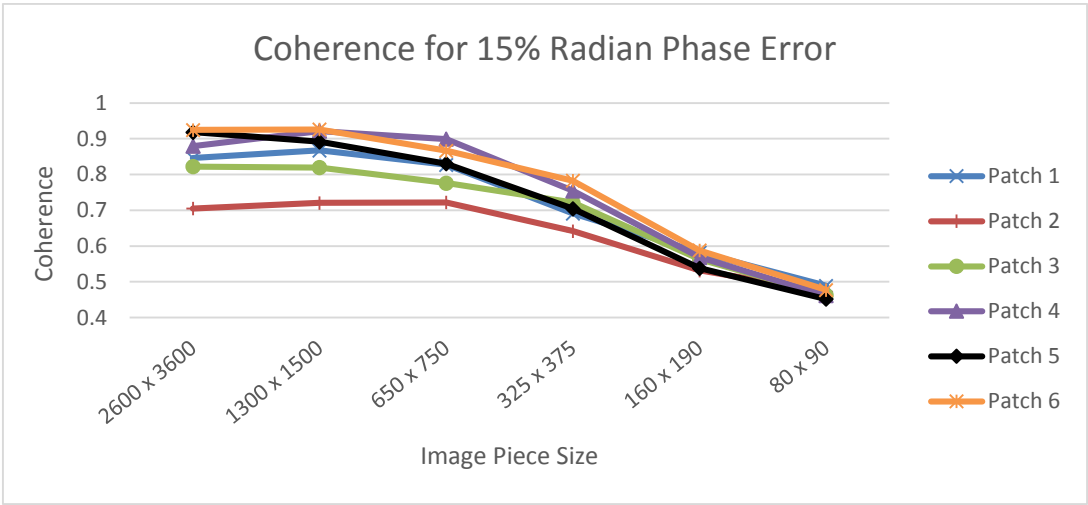


Figure 39: Normalize coherence when a 15% error is applied

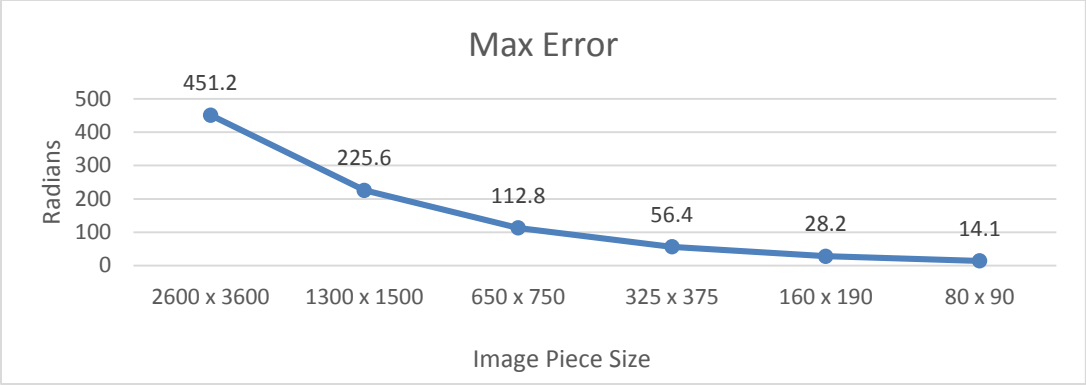


Figure 40: Maximum error applied to each image

Figure 41 shows the 25% phase error caused the coherence to decrease for the largest 2 image piece sizes. This can be contributed to the size of the phase error applied to each of those image piece sizes being too large for PGA. The 4 smaller image piece sizes achieved about the same coherence in the 25% phase error test as the smaller phase error tests.

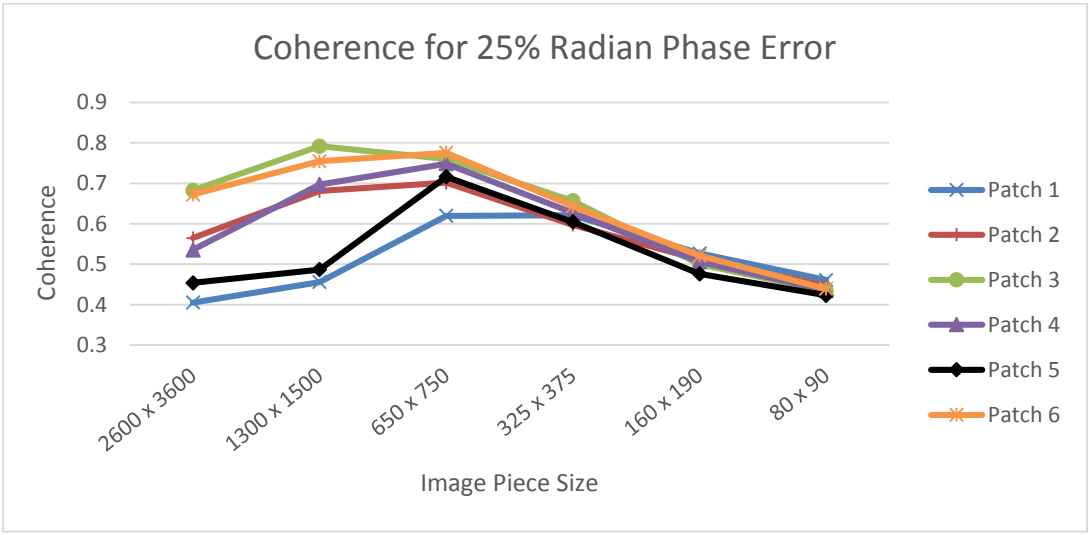


Figure 41: Normalize coherence when a 25% error is applied

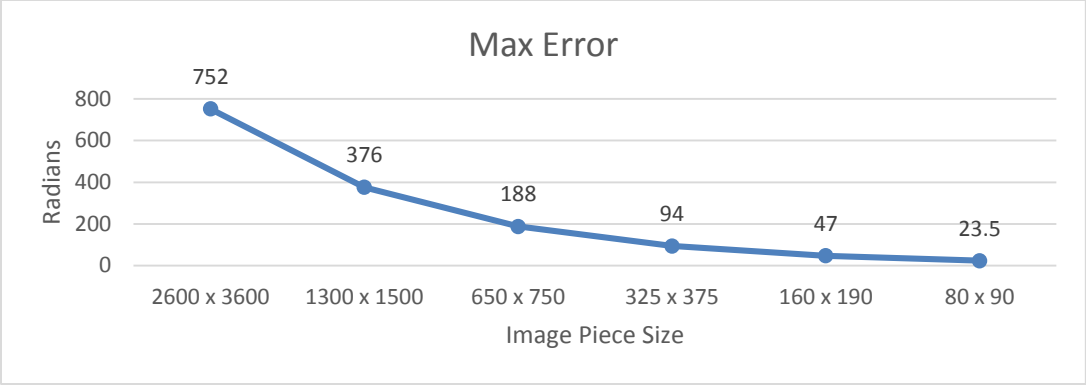


Figure 42: Maximum error applied to each image

## Overall Results

The results from all the coherence figures for the percentage test show that the decline in coherence as image piece size decreases seen in the previous consistent phase error experiment was not because the phase error was too large for the image piece. The decline in coherence as image piece size decreases must be caused by the lack of information in the smaller image pieces. From the data it appears that for PGA to be effective the image size must be greater than the 335 x 375 pixels because around this size the coherence dropped in nearly every test case. If the phase error is large it is best to use the largest image size possible because not only will a larger image be able to focus a large blur footprint but the larger image also has more information which makes PGA's phase error estimate more accurate.

## Preliminary Future Work

Based on the results of the two previous experiments some research was done on image statistics and PGA's performance. Different image pieces from the image shown in Figure *43* were

grouped into high coherence and low coherence categories. Their histograms and statistics were compared.

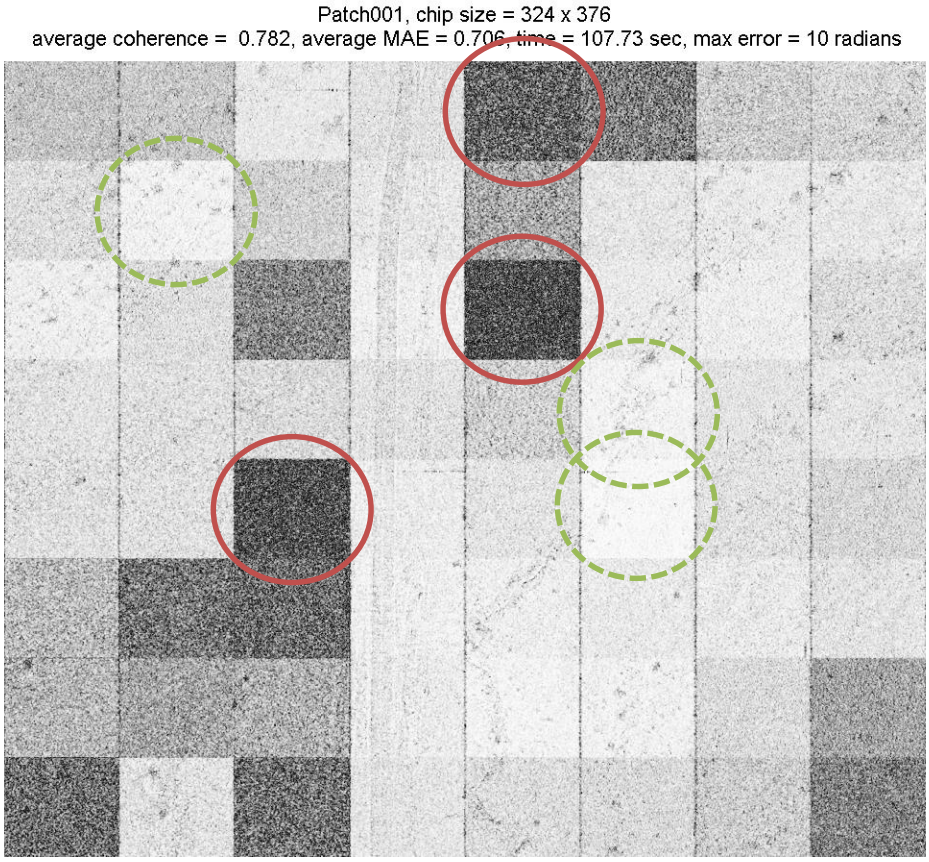


Figure 43 CCD image tested for image statistics

The three pieces shown in the red solid line where grouped into the low coherence category and their histograms are shown in Figure *44*-Figure *46*.

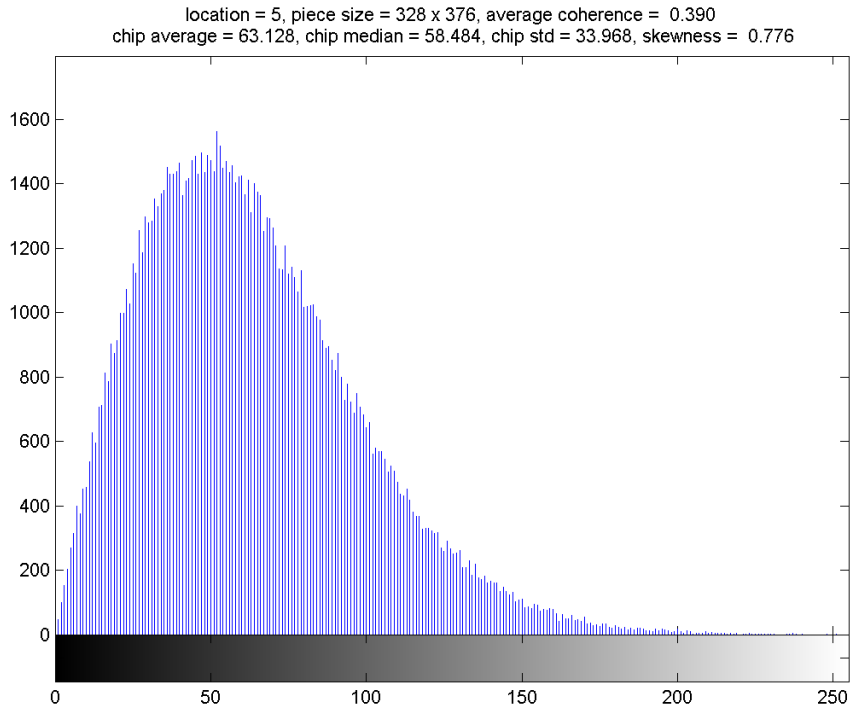


Figure 44: Histogram for piece 5

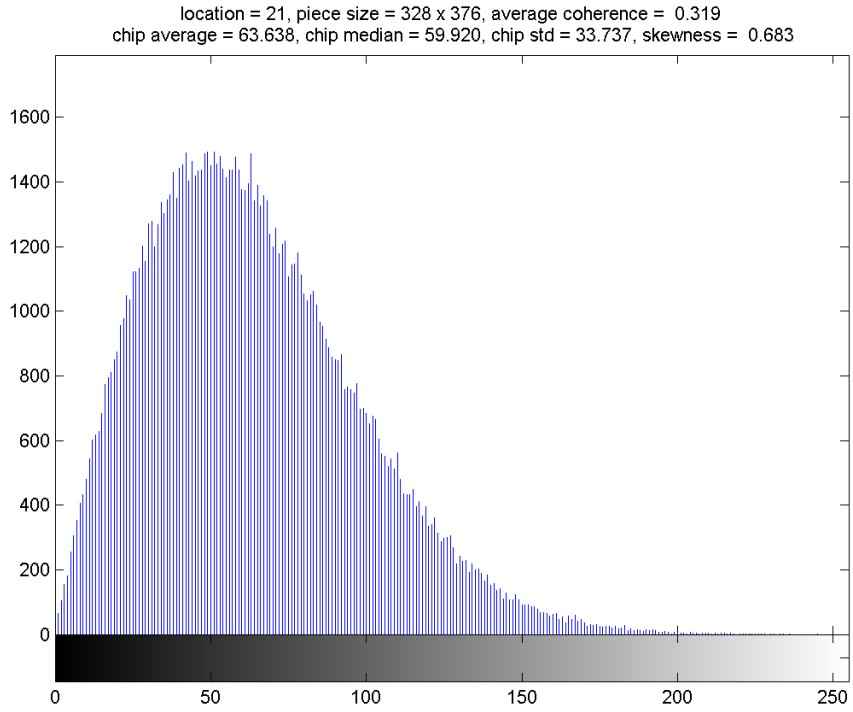


Figure 45: Histogram for piece 21

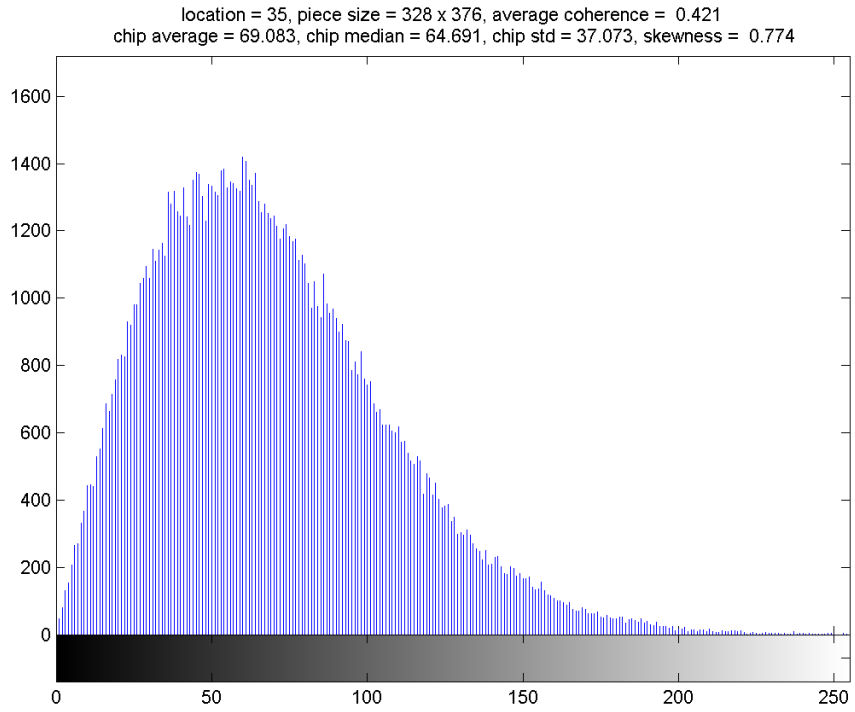


Figure 46: Histogram for piece 35

The three pieces shown in the green dotted circles were grouped into the high coherence category and their histograms are shown in Figure *47*-Figure *49*

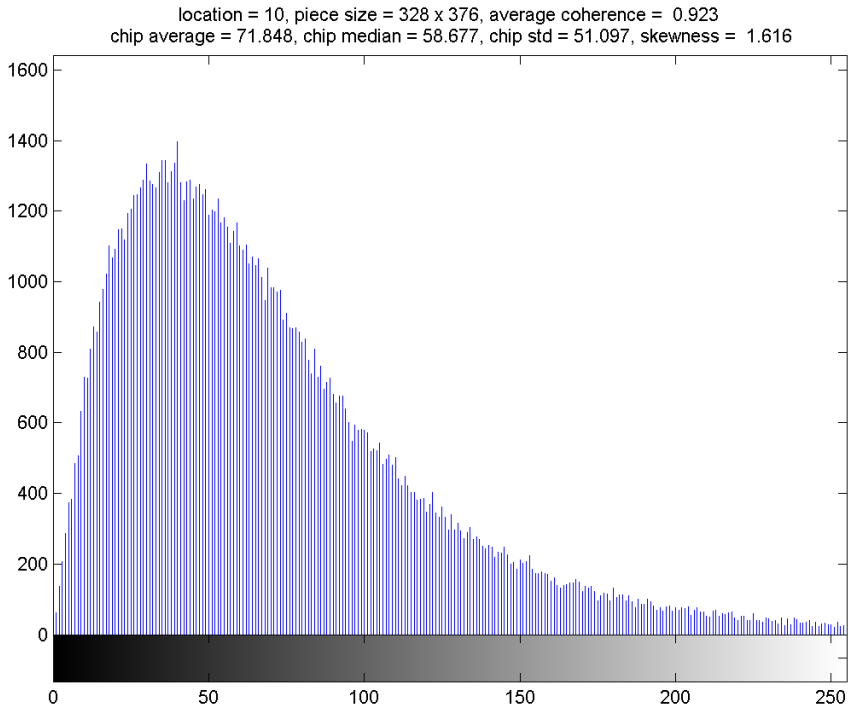


Figure 47: Histogram for piece 10

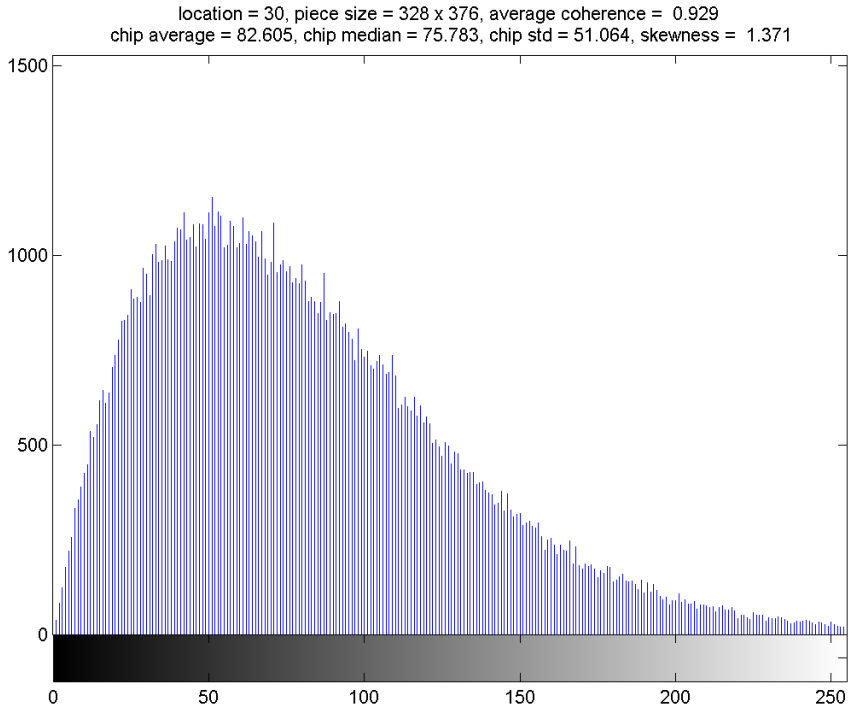


Figure 48: Histogram for piece 30

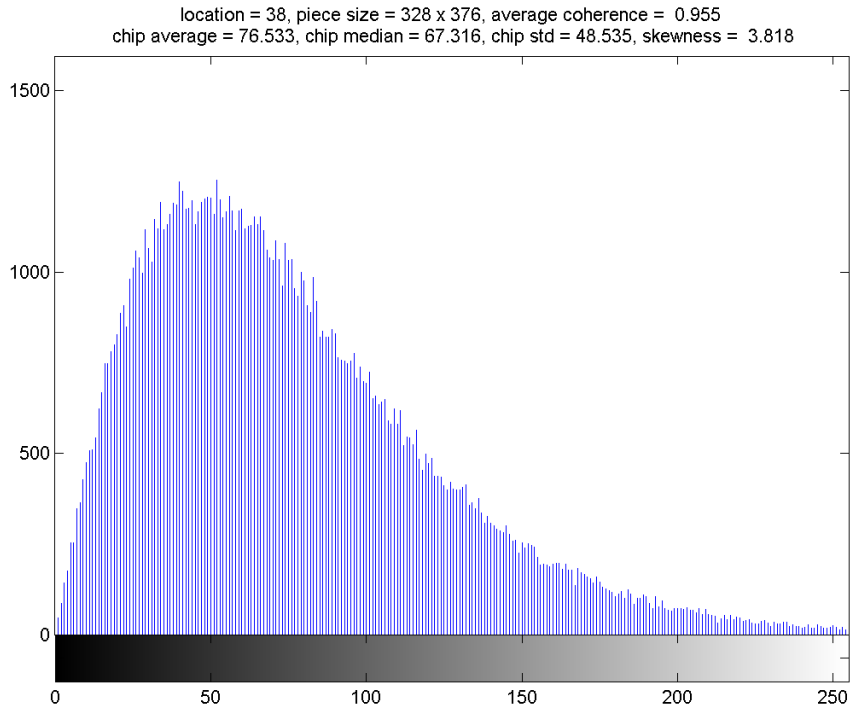


Figure 49: Histogram for piece 38

There does seem to be a relationship between higher coherence and having more high power returns. Skewness could be could be parameters used to predict PGA's performance. Skewness is a measure of a probability distribution's asymmetry about its mean. The skewness of an ideal Rayleigh distribution, the probability distribution of uniform clutter, is .6311. Based on the information gathered from testing the specified image pieces, images with a skewness similar to Rayleigh are more difficult for PGA to focus because they closely resemble uniform clutter. However, further research is needed to test more cases and see if this result is consistent with other images and image sizes.

# CHAPTER V

# CONCLUSION

The purpose of this thesis was to find a minimum image size that can be focused using PGA and the smallest image size tested that still performed well was approximately 650 x 750 pixels. A smaller size could be used if the phase error is less than 20 radians and a larger image size may be needed if the phase error is greater than 200 radians.

There were some instances where the 650 x 750 pixel image failed because of the terrain in that particular image piece. If there are not enough bright point targets for PGA to use to estimate the phase error present in the image PGA will struggle to find the correct error. This is probably the main reason PGA does worse as the image size decreases. When the image size decreases the structure in the image pieces decrease and so do the amount of bright points.

Determining if there is a link between image statistics and PGA performance would also be helpful in determining the minimum size image for PGA. Preliminary tests were done involving mean, median, standard deviation, and skewness of the magnitude of image pieces. Histograms of image pieces were evaluated and the results involving skewness were promising but further research is required.

Further research needs to be done on images from different terrains because of the relationship between image size and terrain. All the images tested were from a similar location and therefore an absolute minimum images size for all regions cannot be draw from this research.

# REFERENCES


[1] C.V. Jakowatz, Jr., D. E. Wahl, P. H. Eichel, D.C. Ghiglia and P. A Thompson, Spotlight-Mode Synthetic Aperture Radar: A Signal Processing Approach. Boston: Kluwer Academic Publisher, 1996.

[2] T. J. Kragh, " Monotonic iterative algorithm for minimum-entropy autofocus," in *Adaptive Sensor Array Processing (ASAP) Workshop]*, 2006.

[3] R. L. Morrison, Jr., M. N. Do, D. C. Nunson, Jr., "MCA: A multichannel Approach to SAR Autofocus," IEEE Transactions on Image Processing, vol. 18, no. 4, pp 840-852, Apr. 2009.

[4] R. L. Morrison, Jr., "Entropy-based autofocus for synthetic aperture radar," M.S. thesis, Dept. Elect. Eng., Univ. Illinois, Urbana-Champaign, 2002.

[5] J. Dunn. "Synthetic Aperture Radar Autofocus: A comparison of phase gradient and minimum entropy algorithms," M.S. thesis, Dept. Elect. Eng., Oklahoma State Univ., Stillwater, OK, 2014.

VITA

Cameron Derek Carroll

Candidate for the Degree of

Master of Science

Thesis: MINIMUM IMAGE SIZE FOR PHASE ERROR CORRECTION USING PHASE GRADIENT AUTOFOCUS ON SYNTHETIC APERTURE RADAR IMAGES

Major Field: Electrical Engineering

Biographical:

Education:

Completed the requirements for the Master of Science in Electrical Engineering at Oklahoma State University, Stillwater, Oklahoma in May 2015.

Completed the requirements for the Bachelor of Science in Electrical Engineering at Oklahoma State University, Stillwater, Oklahoma in December 2015.

Experience:

Electrical Engineering Intern at Sandia National Laboratories (SNL) in Albuquerque, NM, 2014-2015